Identification of proteins involved in *Trypanosoma brucei* DNA replication fork dynamics using nascent DNA proteomics

Maria C Rocha-Granados[1] ¶, Yahaira Bermudez[1]¶, Garvin Dodard[1], Anthula V Vandoros[1], Arthur Günzl[2] and Michele M Klingbeil[1,3]*

[1] Department of Microbiology, University of Massachusetts, Amherst, Massachusetts, United States

[2] Department of Genetics and Genome Sciences, UConn Health, Connecticut, United States

[3] The Institute of Applied Life Sciences, University of Massachusetts, Amherst, Massachusetts, United States

* Corresponding author

Email: klingbeil@microbio.umass.edu

¶These authors contributed equally to this work.

Short title: Trypanosome nascent DNA proteomics

Abstract

DNA replication, transcription and chromatin remodeling are coordinated to ensure accurate duplication of genetic and epigenetic information. In regard to DNA replication, trypanosomatid parasites such as *Trypanosoma brucei* display unusual properties including significantly fewer origins of replication than model eukaryotes, a highly divergent Origin Replication Complex (ORC), and an apparent lack of several replication factor homologs. Although recent studies in *T. brucei* indicate functional links among DNA replication, transcription, and antigenic variation, the underlying mechanisms remain unknown. Here, we adapted an unbiased technology for the identification of replication fork proteins called iPOND (**i**solation of **p**roteins **o**n **n**ascent **D**NA) to *T. brucei*, its first application to a parasite system. This led to the mass spectrometric identification of core replication machinery and of proteins associated with transcription, chromatin organization, and DNA repair that were enriched in the vicinity of an unperturbed active replication fork. Of a total of 410 enriched proteins, among which DNA polymerase α and replication factor C were scoring in the top, around 25% of the proteins identified were of unknown function and, therefore, have the potential to be essential trypanosome-specific replication proteins. Initial characterization of a protein annotated as a Replication Factor C subunit (Tb927.10.7990), and a protein of unknown function (Tb927.3.5370) revealed that both proteins retain nuclear localization throughout the cell cycle. While Tb927.3.5370 appeared to be a dispensable gene, Tb927.10.7990 proved to be essential since its silencing caused a growth defect in procyclic cells, accumulation of zoids and impaired DNA replication. Future studies on the generated proteins list can contribute to the understanding of DNA replication

dynamics in *T. brucei* and how replication is coordinated with other cellular processes to maintain genome integrity.

Introduction

Eukaryotic DNA replication is strictly coordinated and regulated by numerous molecular machines to ensure genomic stability for future cell generations. DNA replication initiation is coordinated with cell cycle progression through the multiprotein Origin Recognition Complex (ORC) that plays an essential role by recruiting proteins that lead to the assembly of the replicative machinery with the assistance of regulatory components Cdc6 and Cdt1. The key factors Cdc45, the MCM replicative helicase complex, and GINS proteins form the CMG complex that further recruits other replication factors such as the clamp loader Replication factor C (RFC), the clamp proliferating cell nuclear antigen (PCNA) and the three replicative DNA polymerases (α, δ, ε) leading to processive DNA replication [1,2].

Instead of the archetypical Origin Recognition Complex (Orc1-6) found in model eukaryotes, trypanosomes contain ORC1 and four other highly divergent ORC subunits (TbORC4, TbORC1b, Tb3120 and Tb7980) [3,4]. Components acting downstream of origin activation are conserved in trypanosomes including the MCM helicase, and portions of the DNA synthetic machinery [5]. However, initiation regulatory factors such as Cdc6 and Cdt1 are lacking, and Cdc45 displays an unorthodox mode of regulation being exported from the nucleus prior to mitosis [4]. Trypanosomes also lack some classical cell cycle checkpoints and it is also well known that there are significant differences in cell cycle regulation between different life cycle stages, although the

74 molecular mechanisms underlying these differences remain elusive [6,7].

75 Additionally, eukaryotic DNA replication is characterized as having multiple
76 origins that are often defined by local DNA structure and chromatin environment rather
77 than by sequence determinants [8–11]. Chromatin environment influences the spatial
78 and temporal distribution of DNA replication events that are also coordinated with
79 transcription. In mouse embryonic cells, 85% of the origins of replication (ORIs) are
80 associated with annotated transcriptional units. Additionally, ORIs with higher firing
81 efficiency are located at CpG islands of promoters [12]. Furthermore, 50% of all
82 activated human ORIs overlap with transcription start sites (TSS), suggesting co-linear
83 progression of DNA replication forks and transcription complexes to prevent head on
84 collisions and potential collapse of the replication fork [13].

85 Evidence for functional interplay between DNA replication and transcription was
86 also found in the trypanosomatid organisms *Leishmania major* and *T. brucei.* In *L.*
87 *major*, ORIs were mapped preferentially at transcription termination sites (TTS),
88 genomic locations where RNA pol II is expected to slow or stall [14].
89 This study concluded that there is coupling between origin activity and transcription,
90 where DNA replication opportunistically initiates from genomic regions that have been
91 available for RNA pol II elongation [14]. A global analysis of DNA replication initiation in
92 *T. brucei* revealed that transcription and DNA replication initiation are coordinated in
93 terms of genomic position [15,16] In *T. brucei*, genes are arranged as polycistronic
94 transcription units also known as directional gene clusters (DGCs). Transcription of
95 DGCs initiates at multiple positions either in divergent strand switch regions (dSSRs) in
96 which DGCs are arranged head-to-head or, in some cases, between two arrays that

face the same direction in a head-to-tail region (HT) [17,18]. dSSRs and HTs are open chromatin regions occupied by acetylated histone H4 (H4K10ac), trimethylated H3 (H3K4me3), histone variants H2A.Z and H2BV, and bromodomain factor 3 [19–22]. The replication initiator protein, TbORC1 prefers the same epigenetic landscape binding to divergent DGCs and the junctions between HT units proximal to H4K10Ac marks. This strong association reveled an unprecedented level of functional interaction between transcription and DNA replication in a eukaryotic genome. How these two machineries are coordinated spatially and temporally remains an open question. Collisions between the replication and transcription machinery are likely more frequent given the large tracks of co-directionally transcribed genes suggesting coordination between the transcription and DNA replication machinery or robust DNA replication restart machinery to overcome fork collapse.

Replication fork dynamics in *T. brucei* have mainly been gene-by-gene investigations that limit studying the machinery in a temporal fashion. The current minimal list of DNA replication factors were identified using biased approaches such as sequence similarity searches based on known replication factors in other model organisms, and affinity purification of associated factors with an already known protein as bait [3,4,23–27] While these studies provided valuable information indicating that the DNA replication machinery differs substantially from its host counterpart, the inventory of DNA replication factors, especially of regulatory factors and trypanosomatid-specific factors, remains incomplete [26].

One technique used to analyze replication fork dynamics and identify the proteins at the replication fork is iPOND (**i**solation of **p**roteins **o**n **n**ascent **D**NA) [28], a method

120 developed in the human system. In iPOND, newly replicated DNA is labeled with the
121 thymidine analog 5-ethynyl-2′-deoxyuridine (EdU) [29]. EdU contains an alkyne
122 functional group that enables the cycloaddition of a biotin azide. This click chemistry
123 reaction [30] yields a stable covalent linkage, facilitating streptavidin capture of cross-
124 linked biotinylated DNA-protein complexes [31]. Combination of the iPOND technology
125 with mass spectrometry (MS) provides a site-specific analysis of replisomes by the
126 identification of the proteins associated to replication forks and helps to determine how
127 these factors are coordinated at the replication site to maintain the genome integrity
128 [32]. iPOND offers an unparalleled ability to identify factors at active and damaged
129 replication forks and to follow the spatial and temporal dynamics of these processes by
130 varying the labeling period with EdU. Additionally, variations using pulse-chase
131 experiments can distinguish between proteins that are specific to replication forks as
132 opposed to proteins that are part of bulk chromatin. Recently, iPOND was adapted in
133 vaccinia virus, the prototype poxvirus, to identify proteins involved in viral DNA
134 replication [33]. In addition to known viral replication proteins, viral DNA-dependent RNA
135 polymerase and transcription initiation and elongation factors were identified on nascent
136 DNA. This suggested that there is temporal coupling of DNA replication and
137 transcription at active replication forks in poxviruses [33].

138 In this study we adapted and applied iPOND technology for the first time in a
139 human-pathogenic parasite, *T. brucei*. By coupling iPOND with label-free mass
140 spectrometric quantification using iBAQ (Intensity-based absolute quantification) [34],
141 we were able to identify 410 proteins that were cross-linked and enriched with nascent
142 DNA. The list includes known replication factors together with DNA repair, transcription,

splicing, and chromatin organization factors. Nearly 25% of the data set were proteins of unknown function. Overall, we obtained a panoramic view of the cellular processes that appear to be coordinated with DNA replication and might help to maintain genomic stability. Additionally, we selected two proteins for initial characterization. These are a putative Replication Factor C subunit (RFC) and a protein of unknown function. Both proteins displayed nuclear localization. Only RFC proved to be essential in PCF cells. Cells in which this protein was depleted exhibited a DNA replication defect and growth impairment.

Materials and Methods

For Primer sequences refer to Supplemental Table 1 (S1 Table).

Plasmid construction

(i) PTP tagging. For PTP allelic tagging of *TbORC1*, *Tb427.03.5370* and *Tb427.10.7990* the C-terminal coding sequence was PCR amplified from *T. brucei* 427 genomic DNA and ligated into either pC-PTP-NEO [35] or pC-PTP-PURO [36]. In pORC1-PTP-NEO, p5370-PTP-NEO and p7990-PTP-PURO the corresponding gene sequences comprised the 3' terminal 1098, 699, and 498 bp of the coding regions, respectively. All final constructs were sequenced. For genome integration, pORC1-PTP-NEO was linearized with SalI, pTb5370-PTP-NEO with AvaI, and pTb7990-PURO with XcmI.

(ii) RNAi. A pStL (stem-loop) vector for inducible gene silencing of each iPOND candidate was constructed as previously described [37]. Briefly, 542 bp or 417 bp of

Tb427.03.5370 or Tb427.10.7990 coding sequence respectively were PCR amplified from *T. brucei* 427 genomic DNA using appropriate primers (S1 Table). Final pStL5370 and pStl7990 vectors were linearized with EcoRV for genome integration.

Trypanosoma brucei **Cell Lines**

Cultivation of the PCF *Trypanosoma brucei brucei* Lister 427 strain [38] and of the 29-13 strain for conditional gene silencing [37] was carried out as described. To generate cell lines expressing PTP-tagged proteins or inducible RNAi, 7.5 μg of linearized plasmid was transfected by nucleofection using an Amaxa nucleofector 2b (Lonza) [39] and cells were selected with either G418, puromycin or phleomycin. In the cell line ORC1$^{PTP/WT}$, the second *TbORC1* allele was deleted using the ApaI/NotI fragment from the pKOORC1-Hyg plasmid and selected using hygromycin [40]. The concentrations of selecting drugs in medium were 50 μg/ml of G418, 1 μg/ml of puromycin, 40 μg/ml of hygromycin and 2.5 μg/ml of phleomycin. Transgenic cell lines were cultured for no more than three weeks. For each transfection, correct DNA integration was confirmed by PCR of genomic DNA with at least one oligonucleotide hybridizing outside of the transfected nucleotide sequence (S1 Table). Conditional gene silencing experiments were performed by incubating trypanosomes in medium containing 1 μg/ml of tetracycline as described [37]. The single expresser clonal cell line ORC1$^{PTP/KO}$ P2C2 (ORC1SE) was used for all iPOND experiments (10 hour doubling time).

Trypanosoma brucei **iPOND**

The original Cortez iPOND method was followed with several modifications [28].

A total of 3 • 10^{10} log phase TbORC1PTP cells were labeled with 150 μM EdU (Santa Cruz) for 10 min. This length of time should label approximately 37 kb of DNA (see calculations in S1 Appendix). In the pulse-chase experiment, EdU labeling was followed by washing of cells once with temperature-equilibrated medium containing 150 μM thymidine and incubation of cells in medium containing 150 μM thymidine for a 60 min chase period prior to pelleting and cross-linking. Cells were pelleted at 3,000 *x g* for 7 min, immediately resuspended at approximately 7.5 • 10^8 cells/ml in SDM-79 medium containing 1.1% formaldehyde, and incubated for 20 min at room temperature (RT) to cross-link DNA-protein complexes. The reaction was quenched by adding 2 M glycine to a final concentration of 0.125 M and incubated for 5 min at RT. Fixed samples were washed three times with cold 1X phosphate buffer saline (PBS), and cell pellets flash frozen and stored at -80°C. For further processing, samples were thawed on ice for 30 min, resuspended with 0.25% Triton-X 100 in PBS in a volume to give an estimated cell density of 1 • 10^9 cells/mL homogenized with 5 passes using a glass dounce, and then incubated for 30 min at RT with gently shaking. Samples were washed once with PBS containing 0.5% BSA and once with PBS, and the pellet was resuspended in click reaction cocktail (0.2 M biotin-azide, 50 mM sodium ascorbate, 10 mM $CuSO_4$) at a volume of 5 ml for every 1 • 10^{10} total cells, and rotated for 2 hours at RT. Following the click reaction, cells were washed as specified above and resuspended in SME buffer (0.25 M sucrose, 10 mM MOPS pH 7.2, 2 mM EDTA, 1 mM PMSF, 1μg/ml leupeptin and one tablet of cOmplete EDTA-free Protease Inhibitor Cocktail (Roche)) containing 0.1% NP40 (cell density of 1 • 10^9 cells/mL). This suspension was homogenized 30 times with a glass dounce and incubated for 1 hour on ice with gentle shaking prior to

211 nitrogen cavitation at 2250 psi (20 min equilibration in SME buffer with 0.1% SDS). If
212 necessary, this step was repeated (1500 psi and 10 min of equilibration) until >85% cell
213 lysis (via microscopy) was achieved. Samples were centrifuged at 1250 *x g* for 10 min
214 to obtain an enriched nuclear fraction (P1, S1 Fig), washed (SME, then PBS) and
215 resuspended in sonication buffer (0.7% wt/vol SDS in 50 mM Tris pH 8.0, 1 μg/ml
216 leupeptin and one tablet of cOmplete EDTA-free Protease Inhibitor Cocktail) by dounce
217 homogenization. Samples were sonicated 5X (10 min, 30s $^{ON/OFF}$) using the Bioruptor
218 UCD-200 (Diagenode), and lysates cleared at 16,000 *x g* for 10 min at 4˚C (Input). To
219 capture biotinylated DNA-protein complexes, the Input sample was diluted with 1
220 volume of PBS, mixed with PBS-equilibrated Streptavidin-agarose beads (250 µl beads
221 slurry) (Novagen), and incubated overnight 4°C (16-20 hours) using a rotator. Beads
222 were pelleted (1,800 *x g*, 3 min, RT) and washed once with streptavidin wash buffer (2%
223 wt/vol SDS, 150 mM NaCl, 50 mM Tris-HCl, pH 7.4), once with 1M NaCl, and twice with
224 streptavidin wash buffer. Each wash step included 5 min of rotation and centrifugation
225 (1,800 *x g*, 1 min, RT). Tubes were changed between washes. Proteins were eluted by
226 incubating the beads at 95°C for 25 min in 2X Laemmli sample buffer. As negative
227 controls, cells were not exposed to EdU but treated with only DMSO, and cells exposed
228 to EdU but treated with the click chemistry cocktail that lacked biotin-azide (C^-) were
229 generated. Three biological replicates were performed for each condition except the
230 pulse-chase experiment where only one experiment was analyzed.
231
232
233

234

235 **DNA Fragmentation Analysis**

236 To analyze the extent of DNA fragmentation after sonication, lysate aliquots (50
237 μl) were subjected to cross-link reversal by adding NaCl to a final concentration of 0.2 M
238 and incubating the samples overnight at 64 ˚C. Subsequently, samples were treated
239 with 10 μl RNase A (20 mg/ml) for 30 min at 37 ˚C followed by Proteinase K (Ambion)
240 treatment for 2 hours at 45 ˚C (20 μl of 0.5 M EDTA, 40 ul of Tris pH 6.7 and 10 ul of
241 Proteinase K). Finally, DNA was prepared by phenol/chloroform extraction and ethanol
242 precipitation, and quantified using a Nanodrop 8000 (Thermo Scientific). DNA samples
243 (100 ng) were separated on a 1.5% agarose gel, stained with ethidium bromide and
244 visualized under UV light.

245

246 **Dot Blot Click Chemistry Efficiency Test**

247 Biotinylated tubulin oligonucleotides (standard curve) and sonicated input fraction
248 DNA (2 μg per replicate) were treated with 1 M NaOH, heated at 55 °C (30 min)
249 followed by addition of 2 M ammonium acetate to remove crosslinks. Oligo DNA and
250 sonicated DNA samples (~100 ng) were spotted onto a nylon membrane (GE
251 healthcare science). Oligo DNA (serially diluted ranging from 0.25 pmol to 16 pmol) was
252 spotted in triplicate and input samples (~100 ng) were spotted in duplicate. Membrane
253 was air-dried and cross-linked (Stratalinker 1800) then immediately placed in blocking
254 solution (20% non-fat milk) for 2 hours at 37˚C. Membrane was then rinsed three times
255 in PBS + 0.1% Tween-20 and incubated with Avidin-HRP (1:3000, Life Technologies)
256 for 30 min (37˚C) followed by 3 washes in PBS + 0.1 % Tween-20, each for 15 min.

257 ImageQuant LAS 4000 mini (GE healthcare science) was used for chemiluminescence
258 detection and data were quantified using ImageJ (version 1.51S). DNA from input
259 fractions of each iPOND condition were quantified by nanodrop.
260
261 **EdU and PTP Immunofluorescence**
262 EdU incorporation for a 10 min pulse was confirmed using the Picolyl azide
263 Toolkit (Life Technologies). Cells were labeled with 150 μM EdU for 10 min, immediately
264 harvested, washed with ice-cold PBS and adhered to poly-L-lysine coated slides (5
265 min). Cells were then fixed in 3% paraformaldehyde (5 min, RT), washed in PBS
266 containing 0.1 M glycine (pH7.4) three times (5 min, RT), and permeabilized with 0.1%
267 Triton X-100 in PBS (5 min, RT). After three additional washes with PBS (5 min, RT),
268 Click chemistry was performed using the Click-iT Plus Alexa Fluor Picolyl Azide Toolkit
269 (Life Technologies) according to manufacturer's directions. Following click incubation for
270 1 hour at RT, cells were washed three times (5 min, PBS) and processed for
271 immunofluorescence. Cells were incubated with anti-protein A antibody (Sigma) diluted
272 1:20,000 in PBS/1% BSA for 60 min, washed three times in PBS/0.1% Tween 20, and
273 incubated with Alexa Fluor 594 goat anti-rabbit antibody diluted 1:250 in PBS/1% BSA
274 for 60 min. DNA was stained with 3 μg/ml 4′-6′-diamidino-2-phenylindole (DAPI), and
275 slides were washed 3 times in PBS prior to mounting in Vectashield (Vector
276 Laboratories). Parasites were visualized and images captured either with a Nikon
277 Eclipse E600 microscope with a cooled CCD Spot-digital camera (Diagnostic
278 Instruments) using a 100X Plan Fluo 1.3 (oil) objective or with a Nikon N-SIM E
279 superresolution microscope equipped with an RCA-Flash 4.0 sCOS camera

(Hamamatsu Photonics) and a CFI SR Apochromate TIRF 100X (NA1.49) objective. Z-stacks (6 μm, 240 nm thickness) were acquired using the NIS-Elements Ar software. Image slices were reconstructed using default software parameters and 3D deconvolution using the automatic method in NSIM modality was applied. Images' brightness and contrast were adjusted using Adobe Photoshop CS4 for presentation in figures.

EdU labeling Quantification

(i) Cell Cycle Analysis. Cells were incubated with 150 μM EdU for 30 min, immediately harvested and processed as described above for EdU immunofluorescence. Cells were then incubated with rat monoclonal antibody YL1/2 (Abcam) (60 min, 1:500 in PBS + 1% BSA), washed three times in PBS + 0.1% Tween 20 and then incubated with Alexa Fluor 594 goat anti-rat, stained with DAPI and mounted as described above. At least 325 cells were scored for each time point. Only intact cells identified by phase contrast were included in the analysis. Cells were classified as EdU+ if fluorescence was detected. Position within the cell cycle was determined based on the kDNA morphology (DAPI staining) and number of basal bodies (YL1/2 staining). YL1/2 recognizes RP2, a protein that localizes to transitional fibers and is therefore a marker only for mature basal bodies [41,42]

(ii) EdU Fluorescence Intensity. Images were acquired using the Nikon E600/Spot digital camera system (described above). Non-saturating exposure times were used and non-adjusted images were analyzed using CellProfiler 3.0.0 [43] to measure EdU pixel intensity. Images were segmented with a DAPI signal to generate masks matching cell

303 nuclei from which the mean EdU signal was calculated. A minimum of 220 EdU positive
304 (EdU+) cells were analyzed from each time point. Data were represented using Prism 7
305 (GraphPad).
306
307 **SDS-PAGE and Western Blot Analysis**
308 Samples were fractionated by SDS-PAGE and transferred overnight to PVDF
309 membrane. For Histone 3 (H3) detection, membranes were blocked in PBS + 3% non-
310 fat milk for two hours and incubated with rabbit H3 antiserum (1:50,000, 0.3% blocking
311 solution) for 2 hours. For mono-, di- and trimethylated H3 at lysine 76 (H3K76)
312 detection, membranes were blocked in PBS + 3% BSA for 2 hours, and incubated with
313 antiserum in 0.3% blocking (H3K76me1, 1:300; H3K76me2, 1:1500; H3K76me3,
314 1:3000) for 2 hours. All H3 antibodies were kindly provided by Christian Janzen.
315 ORC1PTP was detected using peroxidase-anti-peroxidase (PAP) (Sigma, 1:2000), and
316 mtHsp70 was detected using *Crithidia fasciculata* specific antibody (1:10,000, gift from
317 Paul Englund). Following primary antibody incubation, membranes were washed three
318 times (PBS + 0.1% Tween-20) prior to incubation with appropriate horseradish
319 peroxidase conjugated secondary antibodies in corresponding blocking solutions. Signal
320 was detected with Clarity™ ECL Blotting Substrate (NEB) using GE Imagequant LAS
321 4000.
322
323 **RNA Isolation and Quantitative reverse transcription-PCR Analysis.**
324 Total RNA was isolated from $5 \cdot 10^7$ cells with Trizol (Thermo Fisher) according
325 to the manufacturer's specifications. RNA concentration was determined using

Nanodrop, and 100 ng of total RNA was converted to cDNA using the High-Capacity cDNA Reverse Transcription Kit with RNase inhibitor and random primers (Thermo Fisher). qPCR was performed using QuantiNova SYBR Green PCR (Qiagen) with 1 µg of cDNA and 0.2 µM of primer (S1 Table) per reaction with a Stratagene MxPro 3000x thermocycler. All reactions were performed in triplicate. Gene knockdown was normalized with RNA of telomerase reverse transcriptase (TERT) [44].

Mass Spectrometry Sample Preparation and Analysis

Final protein elutions (30 µl) of iPOND experiments were separated by SDS-PAGE. The gel of a complete sample lane was excised in sections and sent for liquid chromatography/tandem mass spectrometry (LC/MS/MS) analysis. Samples were further processed by the Keck Biotechnology Center of Yale University using their standard protocols. Briefly, each sample was resuspended in 25 mM ammonium bicarbonate containing 2.5 ng/µl digestion grade trypsin (Promega) and incubated at 37^{o}C for 14 hours. After digestion, peptides were extracted from gels with two volumes of 80% acetonitrile, 0.1% formic acid for 15 minutes, then dried by speed vacuum. Peptides were dissolved in 30 µl of MS loading buffer (2% acetonitrile, 0.2% trifluoroacetic acid), with 5 µl injected for mass spectrometric analysis. LC/MS/MS acquisition was performed on a Thermo Scientific Q Exactive Plus coupled to a Waters nanoAcquity UPLC system.

For database searching, tandem mass spectra were extracted by Proteome Discoverer version 2.1.1.21 (Thermo Fisher). Charge state deconvolution and deisotoping were not performed. Data were searched in-house using the Mascot

algorithm (version 2.6.0) (Matrix Science, London, UK). Mascot was set up to search a *Trypanosoma brucei* database (version 27, containing Lister strain 427 and TREU927, downloaded from http://tritrypdb.org/tritrypdb/). Search parameters used were trypsin digestion (strict) with up to 2 missed cleavages, peptide mass tolerance of 10 ppm, MS/MS fragment tolerance of 0.02 Da, and variable modifications of methionine oxidation, propionamide adduct to cysteine, and deamidation of asparagine and glutamine.

Scaffold (version Scaffold_4.8.2, Proteome Software Inc.) was used to validate MS/MS based peptide and protein identifications. Peptide identifications were accepted if they could be established at greater than 95.0% probability by the Scaffold Local FDR algorithm. Protein identifications were accepted if they could be established at greater than 99.0% probability and contained at least 2 identified peptides. Protein probabilities were assigned by the Protein Prophet algorithm (Nesvizhskii, 2003). Proteins that contained similar peptides and could not be differentiated based on MS/MS analysis alone were grouped to satisfy the principles of parsimony. Proteins sharing significant peptide sequence were grouped into clusters and were inspected individually.

MS quantification

Protein abundance was estimated using the iBAQ (Intensity-based absolute quantification) value of each protein hit in the four different samples in the Scaffold program. The iBAQ value is based on the sum of all identified peptides intensities matching to a specific protein divided by the number of theoretically peptides observable, yielding an accurate proxy of protein abundance [34]. Proteins were

considered to be enriched when they were identified in at least two of the three biological replicates and fulfilled the following criteria: (i) the protein hit must have a fold change over the No Click control that is equal or higher than 10, (ii) it must have a fold change over the DMSO control that is equal or higher than 1.5, and (iii) the protein should be a nuclear protein as determined by a recent nuclear proteome analysis [46], by the trypanosome genome wide localization resource [47], or have a predicted gene ontology (GO) term associated with a known nuclear protein. The lower fold change values for the DMSO control samples were likely due to the excess biotin azide from the click chemistry step that was incorporated as cofactor for some proteins (S2A Table).

To include proteins in our list that were identified in our nascent DNA analysis but absent in either negative control, e.g. obtained an infinite value (INF) for fold change, we set the fold change value from INF to the highest fold change value obtained in a particular experiment. To estimate a total score in order to rank the protein list the fold change (FC) EdU/No click and the FC EdU/DMSO were standardized to a 0-100 scale in each MS replicate. The average from each FC was calculated and the total score was determined by adding average FC EdU/No click by average FC EdU/DMSO.

Bioinformatic Analysis

UniProt IDs of the proteins identified were acquired using the TriTrypDB database accession numbers [48] (http://www.tritrypdb.org/). However, each protein did not have a UniProt ID. GO term analysis and enrichment was performed using PANTHER classification system [49]. The UniProt IDs list was mapped against the *Trypanosoma brucei* reference list in PANTHER version 13.0 (released version

20171205) with the following selections: analysis type, overrepresentation test; annotation database, PANTHER GO-slim Biological process; and test type, Fisher´s Exact test with False discover rate (FDR) < 0.05. The results were sorted by hierarchically order to observe the enriched functional classes. Analysis of protein interaction networks was performed using STRING database [50]. Only interactions from curated databases and text-mining information were considered (confidence interaction score >0.65). The network was visualized using Cytoscape (version 3.6.0) and interaction groups were manually labeled based on GO term biological process [51].

Protein sequences from selected candidates were analyzed using the NCBI conserved domain database search (CDD) [52] to identify possible functional domains present in proteins of unknown function. Sequences were aligned using Clustal Omega with default parameters [53]. Motif search for Tb5370 was performed using the Eukaryotic Linear Motif (ELM) resource for Functional Sites in Proteins [54] with a cutoff for motif probability of 100.

Results and Discussion

T. brucei DNA replication properties for defining iPOND conditions

To purify proteins that associate with nascent DNA in *T. brucei*, we adapted the original iPOND method developed in the laboratory of Dr. David Cortez (Vanderbilt University) [32]. A major limitation of iPOND is the large amount of starting material needed to recover enough protein for proteomic analysis. Therefore, several aspects of

trypanosome biology were considered when calculating the amount of starting material needed for efficient purification. These parameters included the *T. brucei* genome size (26 Mbp) [5], the duration of S phase (90 min) [55], the percentage of S phase cells in an unsynchronized population (20%-30%) [56], the estimated number of early firing origins, and the PCF *T. brucei* DNA replication rate (3.7 kb/min) [57]. To obtain an approximate equal amount of EdU labeled DNA with that in mammalian iPOND ($2.56 \cdot 10^{13}$ kbp corresponding to 28.1 μg DNA), we calculated that $3 \cdot 10^{10}$ PCF cells were needed ($2.59 \cdot 10^{13}$ kbp) to obtain a comparable amount of labeled DNA (Table 1).

Table 1. Comparison of mammalian and *T. brucei* DNA replication parameters

Parameter	Mammalian cells (293T) [a]	*Trypanosoma brucei* (procyclic form)
Genome size	3000 Mbp[b]	26 Mbp
% of cells in S phase	50%[c]	20%-30%[d]
Replication time	480 min[e]	90 min
Replication rate	1.5 kb/min[f]	3.7 kb/min
~Kbp labeled in 10 min	15	37
Estimate firing forks	2138[g]	78[h]
Kbp labeled/fork	32070	2886
Number of cells	1.6×10^9	3×10^{10}
Cells in S phase	8×10^8	7.5×10^9
Total labeled kbp	2.56×10^{13}	2.16×10^{13}
Total µg labeled DNA	**28.1 µg**	**23.7 µg**
Total µg of DNA	5399.1	854.6
% DNA labeled	0.52%	2.77%

[a]Human embryonic kidney cells [31]
[b] [58]
[c] [59]
[d][56]
[e] [60]
[f][61]
[g][62]
[h]See calculations in S1 Appendix

497 To establish iPOND in *T. brucei*, it was necessary to monitor the preparation of
498 nuclei and the enrichment of nuclear proteins. Since there were no suitable antibodies
499 for this purpose available, we took advantage of a previously established cell line in
500 which the DNA replication initiation protein ORC1 was expressed from one allele with a
501 C-terminal PTP tag [40]. To optimize analysis of ORC1-PTP we further manipulated the
502 cells by knocking out the remaining wild-type allele, thereby generating a single
503 expresser cell line (ORC1SE). We confirmed that the ORC1-PTP protein localized to
504 the nucleus during all cell cycle stages and did not impact the fitness of the cells (S1A
505 Fig). The ORC1SE cell line was used for all iPOND experiments and nuclear
506 enrichment was tracked detecting the tag (S1D Fig).
507

508 ## iPOND Optimization in *T. brucei*

509 Establishing the iPOND method in *T. brucei* required the optimization of several
510 steps including EdU incorporation, click chemistry reaction, cell lysis, and DNA
511 fragmentation (Fig 1A). Compared to mammalian cells where 10 μM EdU is sufficient to
512 label DNA in a 10 min pulse, *T. brucei* PCF required 150 μM EdU to detect EdU-labeled
513 DNA by fluorescence microscopy in the same period (Fig 1B). The lack of high affinity
514 thymidine transporters can explain the higher concentration of EdU required for *T.*
515 *brucei* labeling [63]. The high EdU concentration in our study is in accordance with other
516 *T. brucei* labeling studies in which 100-300 μM EdU was applied for 1 hr to uniformly
517 label the nucleus for studies on PCNA [24,25]. Our conditions, however, resulted in
518 discrete spots that likely represent replication foci (Fig 1B).

519 The iPOND technology relies on click chemistry, which is a copper-catalyzed
520 reaction that allows the cycloaddition of an alkyne functional group (present in EdU) to
521 an azide (conjugated to biotin) yielding a stable covalent bond [64,65]. Based on the
522 higher EdU concentrations for labeling, we optimized the efficiency of the click
523 chemistry reaction in *T. brucei* by increasing the final concentration of biotin azide (200
524 μM) in the reaction cocktail 20-fold compared to mammalian conditions (10 μM). An
525 increased amount of biotin azide was also used for iPOND in mouse embryonic cells
526 [66].

527 Following the cross-linking step, standard lysis conditions resulted in incomplete
528 lysis possibly due to a tightly cross-linked microtubule cytoskeleton [67]. Therefore,
529 nitrogen cavitation was used in combination with detergent treatment to more efficiently
530 lyse the cells (85-100% lysis). Despite the use of detergent in this extra step, we
531 obtained a fraction enriched in seemingly intact nuclei (P1) with little visible
532 contamination of kinetoplasts (mitochondrial DNA in *T. brucei*) or flagella (S1B, C Fig).
533 Accordingly, ORC1-PTP was detected only in the P1 fraction while a mitochondrial
534 matrix marker, Hsp70, was detected in both fractions (S1D Fig).

535 Compared to mammalian iPOND, additional rounds of sonication were required
536 to shear the DNA to fragment sizes of 50-200 bp (Fig 1D), a range recommended for
537 streptavidin capture of the cross-linked DNA-protein complexes. In order to monitor the
538 amount of EdU-labeled DNA from sheared DNA samples (Input), we used a sensitive
539 dot blot assay with a standard curve of biotinylated tubulin oligomers. For EdU pulse (E)
540 experiments, 1.76 pmoles (~0.12 μg of DNA) of biotinylated DNA was detected from the
541 2 μg of DNA that was spotted, while there was no detection in the negative controls (Fig

1C). Biotinylated DNA was also detected in the thymidine chase experiment (S1E Fig). These modifications were critical to achieve approximately 24 µg of EdU-labeled DNA in a 10 min EdU pulse, comparable to the 28 µg regularly obtained in mammalian iPOND. In a 10 min pulse, we should label ~37 kbp. (Table 1). See S1 Appendix for details on calculations for iPOND.

Validation of iPOND

To differentiate between proteins associated with nascent DNA, such as DNA polymerase α and the bulk of chromatin, such as modified histones, we compared iPOND from a 10 min EdU pulse with iPOND from a 10 min EdU pulse followed by a 60 min ThD chase. The short pulse should restrict DNA labeling to the vicinity of the replication fork, while during the ThD chase labeled DNA should have moved away from the fork and undergone chromatin deposition and remodeling. Histone deposition (without modification) is coupled with DNA replication, although the precise timing of deposition is still debated [68,69].

In *T. brucei,* localization of posttranslational-modified histones have been studied during the cell cycle [70,71]. For example, immunolocalization of mono- (H3K76me1) and di-methylated H3 variants (H3K76me2) indicated that these modified histones are detected during mitosis and cytokinesis but not during S phase [70], whereas the H3K76me3 modification occurs during all cell cycle stages [71].

To test whether unmodified or K76-methylated histone H3 was present in our final iPOND eluates we carried out western blot analysis using *T. brucei* specific immune sera. There is minor detection of H3 in the EdU sample while its signal

565 increases in the ThD chase sample (Fig 1E, S2 Fig). Methylated H3 is mainly detected
566 in the ThD chase sample (Fig. 1E). For some EdU samples minor amounts of
567 H3K76me1 can be detected (Fig. 1E), however methylated H3 was rarely detected in
568 the EdU samples (S2 Fig).

569 Quantification of band intensities revealed a 1.5% recovery of total H3 signal in
570 the EdU elution compared to its input signal. In contrast, 13% of the H3 signal was
571 recovered in the chase elution compared to the input. Additionally, the H3K76
572 methylation variants are enriched in the chase sample with an average of 8.5%
573 recovery. H3K76me3 is undetectable in the EdU pulse sample even when increased
574 cell equivalents were loaded and longer exposures analyzed (S2 Fig). Even though
575 H3K76me3 was previously detected in all cell cycle stages, its deposition may not occur
576 on newly replicated DNA, possibly explaining why we could not detect it in our EdU
577 elution (E) (Fig. 1E). These data suggest that in procyclic *T. brucei* deposition of
578 unmodified histones occurs on nascent DNA and posttranslational modifications occur
579 as the DNA moves away from the replication fork. In accordance with this notion,
580 Histone 4 lysine 4 acetylation (H4K4ac) was found to be cell cycle regulated with
581 unmodified H4K4 being highest during S phase [72].
582 Based on these results, it appeared that the differences between the EdU and ThD
583 chase iPOND samples likely represent early replicating conditions for the short pulse
584 and matured chromatin for the chase conditions and, therefore, were suitable for
585 proteomic analyses.
586

587 ## Identification of proteins associated with nascent DNA

Proteins associated with nascent DNA (EdU pulse) from three biological replicates were isolated from gels, trypsin-digested, and analyzed by LC/MS/MS. To minimize the identification of false positives, we employed iBAQ to calculate fold changes (FC) between EdU pulse, negative controls and ThD chase samples (see methods for details). In addition, we restricted our analysis to known or putative nuclear proteins and disregarded proteins that are known standard contaminants of proteomic analyses such as low scoring ribosomal proteins, chaperones and proteins of retrotransposal origin [73]. A final score was calculated taking both the FC EdU/DMSO and the FC EdU/No Click into account (see S2 Appendix for details).

Based on these robust criteria, a total of 410 proteins were found to be enriched on nascent DNA (S2A Table). The genes of 98 proteins were annotated as “hypothetical conserved”, encoding proteins of unknown function (S2B Table). Gene Ontology (GO) enrichment analysis using the tool PANTHER [49] revealed 23 GO terms with >3-fold enrichment and a P-value of <0.001 (Fig 2A, S3 Table). The most abundant types of proteins were those involved in chromatin organization (fold enrichment, 10.7), transcription (9.91), DNA replication (7.43) and pre-mRNA splicing (7.03). To gain additional insight into the proteins enriched on trypanosome nascent DNA, we examined their potential relationships using the STRING database. In a STRING analysis, interactions are derived from multiple sources including curated databases that include known experimental interactions and text mining that incorporates prediction of interactions based on statistical links between proteins [50]. The analysis revealed a network of 9 clusters with abundant interactions between DNA replication

and the DNA repair and nucleic acid metabolism clusters. However, there were also abundant links between DNA replication and transcription clusters (Fig 2B).

As expected, known DNA replication proteins were enriched based on GO term analysis (fold enrichment of 7.43; P-value, $1.4 \cdot 10^{-9}$) (Fig 2A, Table 2, S3 Table). Proteins forming the STRING replication cluster included MCM4 and MCM7 of the heterohexameric MCM complex (replicative helicase), DNA polymerases α (Pol α) and δ (Pol δ) (DNA synthesis), PCNA, replication factor C subunits (processivity), and FEN-1 endonuclease (Okazaki fragment processing). While several homologs of known *T. brucei* replication proteins were identified through iPOND and label free quantification in other systems [32,66], our analysis identified factors that were missing from these studies such as MCM and primase subunits (Table 2).

643 **Table 2. DNA replication proteins identified in *T. brucei* iPOND**

Tb427 Protein ID	Tb927 Protein ID	Product Description	Mol. Weight [kDa]	Ranking Position	Total Score	Identified by Cortez lab[a]	Identified by Ernforns lab[b]
Tb427.08.4880	Tb927.8.4880	DNA polymerase alpha catalytic subunit	152	9	134.02	no	yes
Tb427tmp.01.4070	Tb927.11.12250	DNA replication licensing factor MCM4	93	13	132.20	no	yes
Tb427.10.7990	Tb927.10.7990	ATPase, putative, replication factor 3	39	15	114.68	no	yes
Tb427.03.830	Tb927.3.830	flap endonuclease-1 (FEN-1), putative	44	71	77.62	no	yes
Tb427tmp.01.7810	Tb927.11.16140	DNA replication licensing factor MCM7	81	93	73.57	no	yes
Tb427.03.1130	Tb927.3.1130	DNA polymerase delta subunit 2, putative	62	134	70.40	no	yes
Tb427tmp.01.1310	Tb927.11.9550	replication factor C, subunit 4, putative	38	149	69.20	yes	yes
Tb427tmp.211.3310	Tb927.9.12300	replication factor C, subunit 3, putative	40	180	51.86	no	yes
Tb427.02.1800	Tb927.2.1800	DNA polymerase delta catalytic subunit, putative	117	189	48.39	yes	yes
Tb427.06.3890	Tb927.6.3890	replication factor C, subunit 2, putative	39	216	42.93	yes	yes
Tb427.07.2310	Tb927.7.2310	DNA primase small subunit, putative	48	219	42.80	no	no
Tb427tmp.02.3360	Tb927.11.5650	replication factor C, subunit 1, putative	65	238	41.01	yes	yes
Tb427.04.1330	Tb927.4.1330	DNA topoisomerase IB, large subunit	79	283	37.39	yes	no
Tb427tmp.160.3710	Tb927.9.5190	proliferative cell nuclear antigen (PCNA), putative	32	311	28.61	yes	yes
Tb427.06.4780	Tb927.6.4780	DNA ligase I, putative	83	319	18.60	yes	yes
Tb427tmp.01.0870	Tb927.11.9130	Replication factor A protein 1	52	321	17.37	yes	no
Tb427.05.1700	Tb927.5.1700	replication Factor A 28 kDa subunit, putative	28	388	7.89	no	no

644
645
646 [a][32]
647 [b][66]
648
649

650

651

DNA replication proteins

PCNA, a key component of DNA replication as the sliding clamp, serves as a binding scaffold for numerous replication and DNA damage proteins [74]. In the replication cluster, PCNA was a key node to other DNA replication proteins but also to other clusters (Fig. 2B, purple node). Its interactions with a subunit of the replication factor complex (RFC1; Fig 2B, yellow node), and from RPA (RFA1; Fig 2B, green node), as well as interactions with MCM4 (Fig 2B, pink node) and DNA polymerase α (Pol α; Fig. 2B, red node) were expected. RFC1 is part of the clamp loader involved in PCNA loading, and RFA1 is part of the single-stranded DNA-binding protein complex RPA [75]. *T. brucei* RFC1 and RFA1 were enriched in our data set having ranking positions of 238 and 321 respectively, while PCNA ranked 311 (Table 2, S2A Table). *T. brucei* PCNA shows nuclear localization during the G1/S transition and S phase, regulation of its proper levels is critical for DNA replication and proliferation and is uniquely regulated by the kinase TbERK8 [24,25,27]. MCM4 ranked much higher at 13. The *T. brucei* MCM complex has been characterized and the single MCM4 subunit was able to unwind circular DNA *in vitro* as well as the complex [4].

Interestingly, the most enriched DNA replication protein was the Pol α catalytic subunit (ranking 9) (Table 2; S2A Table). Pol α is recruited to the replication fork after the CMG complex (**C**dc45, **M**CM 2-7 subunits and the **G**INS complex) and activated by MCM10, triggering DNA unwinding at the origin of replication [76,77]. Pol α synthesizes RNA primers and physically interacts with RFC1 and RFA1 at the replication fork [75]. With the exception of PCNA and the MCM subunits, there are no functional studies for the core replication proteins. Some known replication factors did not display high scores

and other known DNA replication proteins did not pass the filtering criteria including DNA polymerase epsilon catalytic subunit, MCM2, Replication Factor A (51 kDa subunit) and DNA topoisomerase II. This is possibly due to low copy numbers of these proteins at the replication fork or less efficient interaction with the DNA.

Several proteins of unknown function are likely to be DNA replication or repair proteins based on the presence of conserved domains. For example, Tb927.3.5370 and Tb927.9.10400 contain regions of similarity to type II DNA topoisomerases. DNA topoisomerases manage the topological state of the DNA, with type II enzymes catalyzing the passage of one double stranded DNA duplex through a break in another DNA duplex in an ATP dependent mechanism [78,79]. A range of processes including DNA replication, DNA repair, sister chromatid segregation, chromosome condensation and catenation rely on type II topoisomerases [80,81].

Another interesting candidate, Tb927.9.15070, has similarity to DNA processing A (DprA) superfamily (NCBI Conserved Domains Database, cl22881). DprA is a bacterial member of the larger, extremely diverse recombination mediator protein (RMP) family. RMPs facilitate binding of RecA-like recombinases (RecA, Rad51) to DNA damage sites for the repair of broken chromosomes and other types of DNA lesions [82].

To test if the DNA replication proteins identified are enriched on nascent DNA, we calculated the FC EdU/ThD chase for these proteins. We compared the ThD chase sample with the three EdU pulse replicates and the FC estimated in each EdU pulse was added to obtain an average FC. From this analysis, RFC4 and MCM4 were only detected in the EdU and absent in the ThD chase sample (INF value). The remaining known DNA replication proteins have a total FC ranging from 0.6 to 4.7, where PCNA is

698 highly enriched (S2C Table) compared to the ThD chase sample. Therefore, DNA
699 replication proteins such as MCM4 and PCNA are in close proximity to the replication
700 fork in the EdU pulse and as the labeled DNA moves away from the fork in the
701 thymidine chase, these proteins are not enriched or are no longer detected. Our results
702 are in agreement with iPOND results from other systems [28,66,83],
703

704 ## Other enriched proteins

705 Our data set revealed DNA repair as a GO term (S2D Table) with a fold
706 enrichment of 5.43 (P-value $8.10 \cdot 10^{-8}$). RAD54 (rank 12) and RAD51 (rank 378)
707 participate in repairing DNA double-strand breaks by homologous recombination and
708 have physical and functional interaction. RAD54 drives branch migration and stimulates
709 RAD51 strand exchange activity [84] whereas RAD51 mediates homology search,
710 strand invasion, and D-loop formation steps [85]. When RAD51 was knocked out in *T.*
711 *brucei*, the parasites were more sensitive to DNA damaging agents [86]. The fact that
712 we are enriching proteins related to DNA repair on nascent DNA might indicate that
713 DNA repair is active during new synthesis or shortly after DNA is replicated.
714 Using SV40 minichromosomes, nucleosomes were shown to assemble
715 immediately behind the DNA replication fork with the first deposited nucleosome
716 detected at a distance of only ~250 bp from the replication fork [87]. An estimated 37
717 kbp of *T. brucei* DNA can be labeled in a 10 min EdU pulse. Therefore, if nucleosome
718 assembly occurs similarly near the active fork, it would be expected to find enrichment
719 of these assembly/remodeling proteins on nascent DNA in *T. brucei*. Accordingly, we
720 found that chromatin organization had the highest fold enrichment (10.70; P-value of

721 $2.91 \bullet 10^{-12}$) (Fig 2A, S3 Table). Nucleosome components such as histone 3 (H3), 4
722 (H4), 2A (H2A), 2B (H2B), 2A variant Z (H2A.Z), 2B variant (H2BV) and 3 variant (H3V)
723 were all detected in the data set (S2A and S2D Tables). H2A.Z and H2BV are
724 specifically deposited at TSSs, whereas H3V was found at TTSs [19]. Histone
725 chaperones such as FACT, contribute to rapid nucleosome assembly at the replication
726 fork, and chromatin remodeling enzymes such as Isw1 help load and position
727 nucleosomes during DNA replication [69]. Accordingly, there are representatives from at
728 least 3 chromatin remodeling complexes present in the data set, namely both FACT
729 subunits (rank 212, 375), two INO80 RuvB-like proteins (rank 338,397), and 3 of the 4
730 ISWI complex proteins (rank 96, 255, 324). In addition, several other putative
731 nucleosome assembly proteins were detected (S2E Table). Interestingly, when
732 comparing average FC EdU/ThD chase, several of the chromatin associated proteins,
733 especially the FACT components, were enriched on nascent DNA further supporting the
734 notion that nucleosome assembly occurs in proximity to the replication
735 fork (S2E Table).

736 There are numerous examples replication and transcription responding to similar
737 cues from the chromatin landscape in eukaryotes. Genome-wide studies in *Drosophila*
738 revealed that early replicating regions were associated with increased transcriptional
739 activity, activating chromatin marks (acetylation), and increased ORC binding, while late
740 replicating regions were associated with repressive histone marks (methylation) [88,89].
741 Genome-wide analyses of *T. brucei* ORC1 binding revealed surprisingly few origins of
742 replication (~100) that map to the boundaries of their DGC revealing an unprecedented
743 level of functional interaction between transcription and DNA replication [15].

744 Additionally, in the related trypanosomatid *L. major*, genome-wide studies indicated that
745 initiation and timing of DNA replication depend on RNA pol II transcription dynamics that
746 also serve as a driving force for nucleosomal organization [14].

747 In support of an intimate association between transcription and DNA replication
748 machineries, the transcription GO term had a 9.91-fold enrichment (P-value of $3.66 \cdot$
749 10^{4}) (Fig 2A; Table 3), and STRING analysis showed transcription proteins interacting
750 with all clusters except for nuclear transport and protein metabolism (Fig 2B). Notably,
751 the main subunits of all three nuclear RNA polymerases were identified which may
752 reflect the facts that RNA pol I in trypanosomes transcribes the genes encoding the
753 parasite's major cell surface proteins [90] and that RNA pol III transcribes genes often
754 located in convergent SSRs [19,91]. A small percentage (7%) of early replicating
755 TbORC1 binding sites are associated with convergent SSRs, and these sites could
756 overlap with RNA Pol III transcription start sites [15,19,91]. Other important transcription
757 proteins identified include TATA-box binding protein (rank 16), two elongation factors
758 (rank 98, 110), and several basal transcription initiation factors (rank 68, 72, 131, 147,
759 240). These findings are in accordance with enrichment of transcription machinery in
760 iPOND studies conducted in other systems [33,66,83].
761
762
763
764
765
766

767 **Table 3. List of Transcription related protein identified in *T. brucei* iPOND**

Tb427 Protein ID	Tb927 Protein ID	Product Description	Mol. Weight [kDa]	Ranking Position	Total Score
Tb427.04.5320	Tb927.4.5320	Component of IIS longevity pathway SMK-1, putative	97	7	134.65
Tb427.10.15950	Tb927.10.15950	TATA-box-binding protein	29	16	109.87
Tb427.10.2780	Tb927.4.5020	DNA-directed RNA polymerase II subunit RPB1	170	29	104.03
Tb427tmp.47.0010	Tb927.11.1390	class I transcription factor A, subunit 1	53	68	78.98
Tb427.01.1700	Tb927.1.1700	AATF protein, putative (Apoptosis-antagonizing transcription factor)	55	69	78.31
Tb427.02.5030	Tb927.2.5030	transcription initiation protein, putative	80	72	77.59
Tb427.01.1680	Tb927.1.1680	Transcription elongation factor 1 domain-containing protein	26	98	73.27
Tb427.04.3510	Tb927.4.3490	DNA-directed RNA polymerases II and III subunit RPB6, putative	16	99	73.21
Tb427.08.5090	Tb927.8.5090	DNA-directed RNA polymerase I largest subunit	196	104	73.03
Tb427tmp.03.0760	Tb927.11.370	repressor activator protein 1	93	105	72.94
Tb427.02.3580	Tb927.2.3580	transcription elongation factor s-II, putative	52	110	72.53
Tb427.08.5980	Tb927.8.5980	TFIIH basal transcription factor complex helicase subunit, putative	92	131	70.54
Tb427tmp.01.5370	Tb927.11.13810	ATP- dependent RNA helicase, putative	63	143	70.00
Tb427tmp.01.1200	Tb927.11.9430	TFIIH basal transcription factor subunit	41	147	69.28
Tb427tmp.02.0970	Tb927.11.3480	Sin-like protein conserved region, putative	79	200	45.94
Tb427.01.540	Tb927.1.540	DNA-directed RNA polymerase III, putative	127	217	42.92
Tb427.10.8720	Tb927.10.8720	CCR4-NOT transcription complex subunit 10, putative	61	236	41.14
Tb427tmp.47.0008	Tb927.11.1410	class I transcription factor A, subunit 3	47	240	40.68
Tb427.10.15370	Tb927.10.15370	DNA-directed RNA polymerases I and III subunit RPAC1, putative	37	242	40.47
Tb427tmp.160.4220	Tb927.9.5710	general transcription factor IIB	38	245	40.30
Tb427.03.1270	Tb927.3.1270	PRP38 family, putative	61	256	39.67
Tb427.04.1310	Tb927.4.1310	ZFP family member, putative zin finger transcription factor	47	294	36.37
Tb427tmp.03.0450	Tb927.11.630	RNA polymerase I second largest subunit	179	323	16.03
Tb427.04.3810	Tb927.4.3810	DNA-directed RNA polymerase II subunit 2, putative	134	336	13.67
Tb427tmp.211.3840	Tb927.9.12900	RNA polymerase-associated protein LEO1, putative	65	354	10.92
Tb05.5K5.70	Tb927.5.4420	nucleolar RNA helicase II, putative	69	380	38.72
Tb427.08.1510	Tb927.8.1510	ATP-dependent RNA helicase DBP2B, putative	62	381	8.68
Tb11.v5.0414	Tb927.10.540	ATP-dependent RNA helicase SUB2, putative	49	407	4.28

768 Interestingly, proteins involved in pre-mRNA splicing were also enriched on
769 nascent DNA (GO term fold enrichment of 7.03 P-value of $2.21 \cdot 10^{-7}$) (Fig 2A,S2F
770 Table). Proteins that are part of the spliceosome such as SmB (rank 42), SmD2 (rank
771 163) and U5-40K (rank 308) were identified. Also, proteins involved in polyadenylation
772 and capping were identified (S2E Table). Recently, the link between nucleosome
773 occupancy, RNA pol II levels and splicing elements in *T. brucei* was addressed [92]. In
774 this study, RNA pol II sites were found in close proximity to regions marked by the
775 histone variant H2A.Z and were associated with TSS. The RNA Pol II enrichment could
776 indicate transcription pausing when encountering nucleosomes and can cause a
777 recruitment of the splicing factors [92]. H2A.Z, RNA pol II subunits and splicing factors
778 are enriched in our data set suggesting that co-transcriptional splicing events might
779 occur in near proximity of newly replicated DNA.
780

781 ## Analysis of Newly Identified Factors.

782 To begin a functional analysis of our data set, we selected the putative replication
783 protein RFC3 (Tb927.10.7990; rank 15) and a protein of unknown function,
784 Tb927.3.5370 (rank 123) that contained a conserved Type II-like topoisomerase
785 domain. To date, there have been no functional studies for any of the RFC subunits.
786 Using TritrypDB resources, Tb7990 appeared to be important for parasite fitness in RIT-
787 seq analysis but showed little change in transcript levels during the cell cycle [93,94]. In
788 contrast, Tb5370 was not greatly affected in RIT-seq but showed cell cycle-dependent
789 changes in transcript levels that peaked during S phase. In the high-throughput TrypTag
790 study [47], both proteins localized to the nucleus.

Tb5370 was selected because of its strong expression during S-phase and its possible association with type II topoisomerases that relieve topological constraints produced in many processes including DNA replication and transcription. The NCBI Conserved Domain Database [52] revealed similarity to a Top2c domain (domain PTZ00108, E-value 5.16 x 10^{-5}). However, protein alignment of Tb5370 with other type II topoisomerases showed Tb5370 was lacking key residues involved in topoisomerase activity. By inspecting for other conserved motifs in Tb5370 and the corresponding homologs in other trypanosomatids, we identified an FHA (forkheaded associated domain) phosphopeptide ligand motif and the cyclin dependent kinases (CDK) phosphorylation site motif (S3 Fig). Importantly, using the phosphoproteomic data available for *T. brucei* [95], three serine residues are phosphorylated in the CDK phosphorylation motif of Tb5370 suggesting it is likely controlled by a kinase (S3 Fig). CDKs phosphorylate protein substrates that are associated with regulation of cell cycle transitions [96], such as DNA synthesis and mitosis [97]. In addition, these kinases also phosphorylates proteins involved in DNA damage [98]. Since Tb5370 is predicted to have FHA motifs which are present in proteins involved in DNA repair and transcription [99], and to be phosphorylated by CDKs, we decided to further evaluate this gene to assess if is essential in *T. brucei*.

Tb7990 was annotated as RFC3. Replication factor C (RFC) is a five-subunit complex that catalyzes the ATP-dependent loading of PCNA onto DNA for replication and repair. The five essential subunits contain the ATP-binding Walker A motif with the consensus sequence GxxxxGKK, the magnesium ion-binding Walker B motif hhhhNExx that is required for ATP hydrolysis [100], and the SRC motif, also called an arginine

finger, that senses bound ATP and participates in ATP hydrolysis [101]. RFC5 subunits differ slightly in having an imperfect Walker B motif that prevents ATP hydrolysis [101]. Tb7990 contains the three conserved motifs (S4 Fig), however Tb7990 has distinct substitutions in the Walker A (GxxxxGKT) and Walker B (hhhhDExx) motifs.

To evaluate the nuclear localization of these proteins during the cell cycle, each factor was fused at the C-terminus with the PTP tag and expressed from their respective endogenous locus in clonal procyclic cell lines. To directly examine localization of the tagged proteins during DNA replication, we labeled bulk DNA with DAPI and newly synthesized DNA with EdU (Fig 3). We applied structured illumination microscopy (SIM) to visualize at high-resolution colocalization of the tagged protein with EdU foci following 10 min of labeling. Both proteins displayed nuclear localization throughout the cell cycle. The Tb5370-PTP signal localized more at the nuclear periphery reminiscent of nuclear pores and did not appear to overlap with EdU foci (Fig 3A). This distinct pattern was retained even during mitosis (data not shown). Tb7990-PTP localized as several punctate foci and was excluded from the nucleolus. While there was colocalization with EdU foci, the two patterns did not precisely overlap, suggesting Tb7990 may have roles other than DNA replication (Fig 3B). There are four different RFC complexes in eukaryotes: RFC1-RFC, Ctf18-RFC, Elg1-RFC and Rad17-RFC [102]. These three complexes share the four small RFC subunits (RFC2, 3, 4, and 5) but differ in the large subunit [103,104]. RFC1-RFC is the canonical RFC complex that acts as a processivity factor for DNA polymerases during replication [105]. Ctf18-RFC is involved in chromatid cohesion [106], Elg1-RFC plays role in genome stability [107] and Rad17-RFC is part of the DNA damage checkpoint response [108].

837 The function of Tb5370 was further explored using a stemloop RNAi construct to
838 deplete its mRNA in a tetracycline-dependent manner. However, there was no loss of
839 fitness following induction of RNAi. Tb5370 RNAi cells before and after tetracycline
840 induction were harvested for RNA isolation and mRNA levels were monitored using RT-
841 qPCR (S5 Fig). *Tb5370* mRNA levels were reduced 80-90% in several clones that were
842 analyzed. It appears that Tb5370 is not essential under standard growth conditions,
843 however a role in DNA repair cannot be ruled out at this point.

844 To further investigate the function of Tb7990, this gene was silenced using
845 inducible RNAi. We prepared total RNA from uninduced and tetracycline-treated cells
846 after 48 hr of growth and monitored mRNA levels using RT-qPCR (Fig 4A, inset).
847 *Tb7990* mRNA levels were reduced ~75% with a corresponding decrease in fitness
848 starting on day 3 (Fig 4A). To characterize the effect of Tb7990 depletion on cell cycle
849 progression and DNA replication directly, cells before and after tetracycline induction
850 were examined using fluorescence microscopy. Since the kinetoplast (K) divides before
851 the nucleus (N), the trypanosome cell cycle stage can be determined by examining
852 DAPI-stained cells in an asynchronous population [56]. Additionally, the appearance of
853 2 mature basal bodies is used to mark the onset of kDNA replication (1N1K*) and is
854 easily visualized using the YL1/2 antibody that is a marker for mature basal bodies. The
855 percentage of cells with 1N1K, 1N1K*, 1N2K and 2N2K configurations were scored (Fig
856 4B, S6 Fig). Tb7990 silencing led to a transient increase in 1N1K* cells, but resulted in
857 an overall decline after 4 days (from 40 to 18%). There was a gradual decline of 1N1K
858 cells (from 42 to 28%) that was accompanied by an increase in 0N1K cells (zoids) from
859 less than 1 to 20% of the population. Cells with other abnormal configurations also

increased by day 5 (from 0 to 12%). Thus, these data indicate that silencing Tb7990 resulted in impaired cell cycle progression. It is important to note that in procyclic *T. brucei*, cell division can proceed in the absence of nuclear division or even nuclear S phase to give rise to anucleate cells (zoids) [109–111]. Additionally, the appearance of zoids and disruption of cell cycle progression was reported for silencing of the DNA replication initiation proteins TbORC1 and MCM subunits [4,40].

To directly test whether Tb7990-depleted cells were defective in DNA replication, the same cells were metabolically labeled with EdU following the induction of Tb7990 dsRNA, and nascent DNA was detected by indirect immunofluorescence microscopy. Cells were scored for the absence (EdU-) or presence (EdU+) of EdU labeling. In an asynchronous uninduced population, 41.1% of the cells exhibited an EdU-dependent fluorescence signal (EdU+) with the great majority of cells being 1N1K* (40.2%). Following Tb7990 depletion, there was an initial increase in the percentage of EdU+ cells that subsequently declined to 26% at Day 5. The percentage of EdU+ 1N1K* cells decreased while the percentage of EdU+ 1N2K cells increased indicating that progression through S phase was impaired and cells were not progressing through mitosis to G2 (Fig 4B, S6 Fig).

In addition to the overall decline in EdU+ cells, the fluorescence intensity of the EdU+ cell population also decreased following 5 days of Tb7990 silencing (S6 Fig). To evaluate statistical significance, we used CellProfiler [43] to score fluorescence intensity in at least 220 EdU+ cells for each time point (Fig 4C). In uninduced cells, there is a distribution of fluorescence intensity ranging from 0.055-0.20 representing cells at the various phases of DNA replication in an unsynchronized population. Interestingly, there

was an increase in fluorescence intensity observed at Day 3 in which the mean intensity increased and the range was broader (0.064-0.28) compared to uninduced (P-value <0.0001). During this time point some of the highest EdU fluorescence intensities were recorded and this timepoint corresponded to an increase in 1N2K cells as well as the percentage of 1N2K cells that were EdU+. By the last day of the RNAi induction, the mean EdU fluorescence intensity decreased even below uninduced values and had the lowest intensities as well as the lowest range (0.011-0.18) compared to all days (D3/D5 P-value <0.0001; Un/D5 P-value <0.02). Together these data demonstrate a role in DNA replication by both a reduction in the number of EdU+ cells and decreases in EdU incorporation.

The Tb7990 RNAi DNA replication defect was similar to the defects reported for silencing *T. brucei* ORC1, MCM subunits (3, 5 and 7) and PCNA in procyclic cells [4,25,40]. Knockdowns of these genes led to a gradual decline in the number of 1N1K cells that was accompanied by a gradual increase in zoid cells (0N1K) and a subtle increase in the 1N2K population, although there was variation in the percentages of cells at each of these cell stages. The accumulation of 1N2K cells can be the result of incomplete mitosis (a nuclear segregation defect) or some perturbation of S phase preventing the cells from initiating mitosis. Both defects can result in progeny where one cell receives some proportion of nuclear material while the other cell receives only a kinetoplast (zoid) (Fig 4D) due to the lack of a classical mitosis to cytokinesis checkpoint in procyclic trypanosomes [109–111]. The combined accumulation of zoids and transient increase in 1N2K cells appears to be a hallmark of DNA replication defects.

Conclusion

Here, we have established the iPOND technology, for the first time in a parasitic system. It is a powerful tool that provided a global view of proteins that are enriched at nascent DNA under unperturbed replication conditions in *T. brucei* PCF cells. Our data suggest that DNA replication, transcription, chromatin organization and pre-mRNA splicing events all occur on and or near nascent DNA. These different cellular processes may be coordinated or just occur in the vicinity of each other. Based on our observations, we propose nucleosomes are assembled close to the replication fork followed by RNA pol II recruitment, transcription, and co-transcriptional RNA processing. Further studies are needed to determine how these processes are linked and co-regulated, and how rapidly they are initiated during DNA replication.

In addition, our data set has provided a list of proteins of unknown function that can be characterized to determine their function in DNA replication and/or at nascent DNA. They could represent essential trypanosomatid-specific factors or extremely divergent homologues of known replication factors and, therefore, represent promising targets of chemotherapeutic intervention. The initial characterization of the protein candidate Tb7990, a replication factor C subunit, indicated an essential role in DNA replication that was quantified using EdU incorporation and microscopy assays.

However, many of the DNA replication proteins identified in our data set have not been studied and their future characterization using our strategy to detect replication defects will contribute to the understanding of DNA replication in *T. brucei*.

Acknowledgements

This work was partially supported by a UMass Graduate School Grant to MCR, and a Faculty Research Grant to MMK. NIH grant AI126455 to MMK supported this work.

We thank David Cortez and Jared Nordman for discussions and ideas. We are grateful to Christian Janzen for providing the H3 antibodies, Paul Englund for the mtHsp70 antibodies, and Bibo Li for the pKOORC1-Hyg plasmid. The superresolution microscopy data were gathered in the Light Microscopy Facility Nikon center of Excellence at the Institute for Applied Life Sciences, UMass Amherst, with support from the Massachusetts Life Sciences center.

Figure Legends

Figure 1. Optimization of iPOND in *T. brucei*. (A) Schematic overview of modified iPOND procedure for *T. brucei*. Red, modifications that were implemented compared to the original iPOND protocol performed in mammalian cells. **(B)** EdU incorporation in newly synthesized DNA in *T. brucei*. In a 10 min EdU pulse, newly synthesized DNA was successfully labeled. DNA is stained with DAPI. Size bar 5 □m. **(C)** Quantification of biotinylated DNA. Biotin incorporation was measured in sonicated samples (input) from negative controls (DMSO; D and Click-; C-), ThD chase (T), and EdU pulse (E) samples. Approximately 2 □g of DNA from sonicated samples (input) were applied to a Hybond membrane. Biotinylated DNA was detected using Avidin HRP. Graph, standards (blue circles) and EdU sample (red square) were plotted. **(D)** DNA fragmentation analysis. 5 cycles of sonication yielded DNA fragments between 50 bp to 200 bp, 100 bp fragments are enriched in all iPOND conditions. **(E)** Detection of Histone 3. H3 was used as a DNA-bound protein marker. Input (In) and final elution (Elu) fractions were probed against H3 and one, two and tree methylation groups present H3 Lysine 76 (H3K76met) in the four iPOND conditions.

Figure 2. Gene ontology enrichment and protein network in *T. brucei* iPOND. (A) PANTHER Gene ontology (GO) analysis of the proteins identified on nascent DNA. Graph represents the fold enrichment of each GO term in a hierarchy order. Only GO terms with a fold enrichment above 3 were plotted. **(B)** Panoramic landscape of the protein–protein interaction network analysis of an active replication fork in *T. brucei* defined by STRING. Relevant interactions and most representative groups are displayed. The topology is organized according to functional classification. Highlighted nodes: DNA polymerase α, red; Replication Factor C, yellow; Replication Factor A subunit 1, green; MCM4, pink; and PCNA, purple.

Figure 3. Intranuclear localization of two iPOND candidates. Localization of PTP-tagged proteins in asynchronous populations labeled with EdU using SIM microscopy. PTP tag was detected with anti-protein A (red), EdU incorporation (green) and DNA was stained with DAPI (blue). Enlargements correspond to the white dashed boxes. **(A)** Tb5370-PTP tagged cell line **(B)** Tb7990-PTP tagged cell line. Size bar, 5 μm.

Fig 4. Silencing of Tb7990 by RNAi. (A) Tb7990 Growth curves, in the presence and absence of tetracycline. Inset, qPCR **(B)** Quantification of cell cycle stages following Tb7990 RNAi. Cells were induced for RNAi (0 – 5 days), EdU labeled for 10 min, fixed, and processed for detection of EdU, basal bodies and DNA. Cells (~325/day) were scored by fluorescence microscopy according to the number of kinetoplasts (K) and nuclei (N), EdU+ nuclei, and number of basal bodies. Some categories (e.g. 2N0K, 2N1K, multiple nuclei) comprised <2% of the total and grouped as Other. Images show examples of each cell type scored and key to bar graphs. **(C)** Each dot represents the mean EdU signal per nucleus for each condition after a 30 min pulse with 150 μM EdU.

(D) Model for production of zoids (adapted from [112]). Larger circles, nuclei; small ovals, kDNA; black, EdU-; green, EdU+.

References

1. Fragkos M, Ganier O, Coulombe P, Méchali M. DNA replication origin activation in space and time. Nat Rev Mol Cell Biol. Nature Publishing Group; 2015;16: 360–374. doi:10.1038/nrm4002
2. Snedeker J, Wooten M, Chen X. The Inherent Asymmetry of DNA Replication. Annu Rev Cell Dev Biol Annu Rev Cell Dev Biol. 2017;33: 291–318. doi:10.1146/annurev-cellbio-100616
3. Tiengwe C, Marcello L, Farr H, Gadelha C, Burchmore R, Barry JD, et al. Identification of ORC1/CDC6-interacting factors in trypanosoma brucei reveals critical features of origin recognition complex architecture. PLoS One. 2012;7: 22–24. doi:10.1371/journal.pone.0032674
4. Dang HQ, Li Z. The Cdc45 Mcm2-7 GINS protein complex in trypanosomes regulates DNA replication and interacts with two Orc1-like proteins in the origin recognition complex. J Biol Chem. 2011;286: 32424–32435. doi:10.1074/jbc.M111.240143
5. Berriman M, Ghedin E, Hertz-Fowler C, Blandin G, Renauld H, Bartholomeu DC, et al. The genome of the African trypanosome Trypanosoma brucei. Science. 2005;309: 416–422. doi:10.1126/science.1112642
6. Hammarton TC. Cell cycle regulation in Trypanosoma brucei. Mol Biochem Parasitol. Elsevier B.V.; 2007;153: 1–8. doi:10.1016/j.molbiopara.2007.01.017
7. Qing Z, Hu H, Li Z. New Insights into the Molecular Mechanisms of Mitosis and Cytokinesis in Trypanosome. Int Rev Cell Mol Biol. 2014. doi:10.1016/B978-0-12-800097-7.00004-X.New
8. Cayrou C, Coulombe P, Vigneron A, Stanojcic S, Ganier O, Peiffer I, et al. Genome-scale analysis of metazoan replication origins reveals their organization in specific but flexible sites defined by conserved features. Genome Res. 2011;21: 1438–1449. doi:10.1101/gr.121830.111
9. Kanter DM, Bruck I, Kaplan DL. Mcm subunits can assemble into two different active unwinding complexes. J Biol Chem. 2008;283: 31172–31182. doi:10.1074/jbc.M804686200
10. Costa A, Hood I V., Berger JM. Mechanisms for Initiating Cellular DNA Replication. Annu Rev Biochem. 2013;82: 25–54. doi:10.1146/annurev-biochem-052610-094414
11. Kurat CF, Yeeles JTP, Patel H, Early A, Diffley JFX. Chromatin Controls DNA Replication Origin Selection, Lagging-Strand Synthesis, and Replication Fork Rates. Mol Cell. Elsevier Inc.; 2017;65: 117–130. doi:10.1016/j.molcel.2016.11.016
12. Sequeira-Mendes J, Díaz-Uriarte R, Apedaile A, Huntley D, Brockdorff N, Gómez M. Transcription initiation activity sets replication origin efficiency in mammalian cells. PLoS Genet. 2009;5. doi:10.1371/journal.pgen.1000446

13. Langley AR, Gräff S, Smith JC, Krude T. Genome-wide identification and characterisation of human DNA replication origins by initiation site sequencing (ini-seq). Nucleic Acids Res. 2016;44: 10230–10247. doi:10.1093/nar/gkw760
14. Lombraña R, Alvarez A, Fernandez-Justel JM, Almeida R, Poza-Carrion C, Gomes F, et al. Transcriptionally Driven DNA Replication Program of the Human Parasite Leishmania major. Cell Rep. 2016;16: 1774–1786. doi:10.1016/j.celrep.2016.07.007
15. Tiengwe C, Marcello L, Farr H, Dickens N, Kelly S, Swiderski M, et al. Genome-wide analysis reveals extensive functional interaction between DNA replication initiation and transcription in the genome of trypanosoma brucei. Cell Rep. Elsevier; 2012;2: 185–197. doi:10.1016/j.celrep.2012.06.007
16. Tiengwe C, Marques CA, McCulloch R. Nuclear DNA replication initiation in kinetoplastid parasites: New insights into an ancient process. Trends Parasitol. Elsevier Ltd; 2014;30: 27–36. doi:10.1016/j.pt.2013.10.009
17. Martínez-Calvillo S, Yan S, Nguyen D, Fox M, Stuart K, Myler PJ. Transcription of Leishmania major Friedlin chromosome 1 initiates in both directions within a single region. Mol Cell. 2003;11: 1291–1299. doi:10.1016/S1097-2765(03)00143-6
18. Kolev NG, Franklin JB, Carmi S, Shi H, Michaeli S, Tschudi C. The transcriptome of the human pathogen Trypanosoma brucei at single-nucleotide resolution. PLoS Pathog. 2010;6: 1–15. doi:10.1371/journal.ppat.1001090
19. Siegel TN, Hekstra DR, Kemp LE, Figueiredo LM, Lowell JE, Fenyo D, et al. Four histone variants mark the boundaries of polycistronic transcription units in Trypanosoma brucei. Genes Dev. 2009;23: 1063–1076. doi:10.1101/gad.1790409.7
20. Daniels J-P, Gull K, Wickstead B. Cell Biology of the Trypanosome Genome. Microbiol Mol Biol Rev. 2010;74: 552–569. doi:10.1128/MMBR.00024-10
21. Siegel TN, Gunasekera K, Cross GAM, Ochsenreiter T. Gene expression in Trypanosoma brucei: Lessons from high-throughput RNA sequencing. Trends Parasitol. Elsevier Ltd; 2011;27: 434–441. doi:10.1016/j.pt.2011.05.006
22. Wright JR, Siegel TN, Cross GAM. Histone H3 trimethylated at lysine 4 is enriched at probable transcription start sites in Trypanosoma brucei. Mol Biochem Parasitol. Elsevier B.V.; 2010;172: 141–144. doi:10.1016/j.molbiopara.2010.03.013
23. De Melo Godoy PD, Nogueira-Junior LA, Paes LS, Cornejo A, Martins RM, Silber AM, et al. Trypanosome prereplication machinery contains a single functional Orc1/Cdc6 protein, which is typical of archaea. Eukaryot Cell. 2009;8: 1592–1603. doi:10.1128/EC.00161-09
24. Kaufmann D, Gassen A, Maiser A, Leonhardt H, Janzen CJ. Regulation and spatial organization of PCNA in Trypanosoma brucei. Biochem Biophys Res Commun. Elsevier Inc.; 2012;419: 698–702. doi:10.1016/j.bbrc.2012.02.082
25. Valenciano AL, Ramsey AC, Mackey ZB. Deviating the level of proliferating cell nuclear antigen in trypanosoma brucei elicits distinct mechanisms for inhibiting proliferation and cell cycle progression. Cell Cycle. 2015;14: 674–688. doi:10.4161/15384101.2014.987611
26. da Silva MS, Pavani RS, Damasceno JD, Marques CA, McCulloch R, Tosi LRO,

et al. Nuclear DNA Replication in Trypanosomatids: There Are No Easy Methods for Solving Difficult Problems. Trends Parasitol. Elsevier Ltd; 2017;33: 858–874. doi:10.1016/j.pt.2017.08.002

27. Valenciano AL, Knudsen GM, Mackey ZB. Extracellular-signal regulated kinase 8 of Trypanosoma brucei uniquely phosphorylates its proliferating cell nuclear antigen homolog and reveals exploitable properties. Cell Cycle. Taylor & Francis; 2016;15: 2827–2841. doi:10.1080/15384101.2016.1222340
28. Sirbu BM, Couch FB, Feigerle JT, Bhaskara S, Hiebert SW, Cortez D. Analysis of protein dynamics at active , stalled , and collapsed replication forks. Genes Dev. 2011;25: 1320–1327. doi:10.1101/gad.2053211.Venkitaraman
29. Salic A, Mitchison TJ. A chemical method for fast and sensitive detection of DNA synthesis in vivo. Proc Natl Acad Sci U S A. 2008;105: 2415–2420. doi:10.1073/pnas.0712168105
30. Kolb HC, Finn MG, Sharpless KB. Click Chemistry: Diverse Chemical Function from a Few Good Reactions. Angew Chem Inte Ed. 2001;40: 2004–2021. doi:10.1002/1521-3773(20010601)40:11<2004::AID-ANIE2004>3.0.CO;2-5
31. Sirbu BM, Couch FB, Cortez D. Monitoring the spatiotemporal dynamics of proteins at replication forks and in assembled chromatin using isolation of proteins on nascent DNA. Nat Protoc. Nature Publishing Group; 2012;7: 594–605. doi:10.1038/nprot.2012.010
32. Sirbu BM, McDonald WH, Dungrawala H, Badu-Nkansah A, Kavanaugh GM, Chen Y, et al. Identification of proteins at active, stalled, and collapsed replication forks using isolation of proteins on nascent DNA (iPOND) coupled with mass spectrometry. J Biol Chem. 2013;288: 31458–31467. doi:10.1074/jbc.M113.511337
33. Senkevich TG, Katsafanas GC, Weisberg A, Olano LR, Moss B. Identification of vaccinia virus replisome and transcriptome proteins by isolation of proteins on nascent DNA coupled with mass spectrometry. J Virol. 2017;91: 1–20. doi:10.1128/JVI.01015-17
34. Schwanhüusser B, Busse D, Li N, Dittmar G, Schuchhardt J, Wolf J, et al. Global quantification of mammalian gene expression control. Nature. 2011;473: 337–342. doi:10.1038/nature10098
35. Schimanski B, Nguyen TN, Gu A. Highly Efficient Tandem Affinity Purification of Trypanosome Protein Complexes Based on a Novel Epitope Combination. Eukaryot Cell. 2005;4: 1942–1950. doi:10.1128/EC.4.11.1942
36. Bruhn DF, Mozeleski B, Falkin L, Klingbeil MM. Mitochondrial DNA polymerase POLIB is essential for minicircle DNA replication in African trypanosomes. Mol Microbiol. 2010;75: 1414–1425. doi:10.1111/j.1365-2958.2010.07061.x
37. Chandler J, Vandoros A V., Mozeleski B, Klingbeil MM. Stem-loop silencing reveals that a third mitochondrial DNA polymerase, POLID, is required for kinetoplast DNA replication in trypanosomes. Eukaryot Cell. 2008;7: 2141–2146. doi:10.1128/EC.00199-08
38. Concepción-Acevedo J, Luo J, Klingbeil MM. Dynamic localization of Trypanosoma brucei mitochondrial DNA polymerase ID. Eukaryot Cell. 2012;11: 844–55. doi:10.1128/EC.05291-11
39. Sakyiama J, Zimmer SL, Ciganda M, Williams N, Read LK. Ribosome biogenesis

requires a highly diverged XRN family 5'->3' exoribonuclease for rRNA processing in Trypanosoma brucei. Rna. 2013;19: 1419–1431. doi:10.1261/rna.038547.113

40. Benmerzouga I, Concepción-Acevedo J, Kim HS, Vandoros A V., Cross GAM, Klingbeil MM, et al. Trypanosoma brucei Orc1 is essential for nuclear DNA replication and affects both VSG silencing and VSG switching. Mol Microbiol. 2013;87: 196–210. doi:10.1111/mmi.12093
41. Harmer J, Qi X, Toniolo G, Patel A, Shaw H, Benson FE, et al. Variation in Basal Body Localisation and Targeting of Trypanosome RP2 and FOR20 Proteins. Protist. Elsevier GmbH.; 2017;168: 452–466. doi:10.1016/j.protis.2017.07.002
42. Andre J, Kerry L, Qi X, Hawkins E, Drižyte K, Ginger ML, et al. An alternative model for the role of RP2 protein in flagellum assembly in the African trypanosome. J Biol Chem. 2014;289: 464–475. doi:10.1074/jbc.M113.509521
43. Carpenter AE, Jones TR, Lamprecht MR, Clarke C, Kang IH, Friman O, et al. CellProfiler: image analysis software for identifying and quantifying cell phenotypes. Genome Biol. 2006;7. doi:10.1186/gb-2006-7-10-r100
44. Brenndörfer M, Boshart M. Selection of reference genes for mRNA quantification in Trypanosoma brucei. Mol Biochem Parasitol. 2010;172: 52–55. doi:10.1016/j.molbiopara.2010.03.007
45. Nesvizhskii AI, Keller A. A statistical model for identifying proteins by tandem mass spectrometry. Anal Chem. 2003;75: 4646–4658. doi:10.1021/ac0341261
46. Goos C, Dejung M, Janzen CJ, Butter F, Kramer S. The nuclear proteome of Trypanosoma brucei. PLoS One. 2017;12: e0181884. doi:10.1371/journal.pone.0181884
47. Dean S, Sunter JD, Wheeler RJ. TrypTag.org: A Trypanosome Genome-wide Protein Localisation Resource. Trends Parasitol. Elsevier Ltd; 2017;33: 80–82. doi:10.1016/j.pt.2016.10.009
48. Aslett M, Aurrecoechea C, Berriman M, Brestelli J, Brunk BP, Carrington M, et al. TriTrypDB: A functional genomic resource for the Trypanosomatidae. Nucleic Acids Res. 2009;38: 457–462. doi:10.1093/nar/gkp851
49. Mi H, Muruganujan A, Casagrande JT, Thomas PD. Large-scale gene function analysis with the panther classification system. Nat Protoc. 2013;8: 1551–1566. doi:10.1038/nprot.2013.092
50. Szklarczyk D, Franceschini A, Wyder S, Forslund K, Heller D, Huerta-Cepas J, et al. STRING v10: Protein-protein interaction networks, integrated over the tree of life. Nucleic Acids Res. 2015;43: D447–D452. doi:10.1093/nar/gku1003
51. Smoot ME, Ono K, Ruscheinski J, Wang PL, Ideker T. Cytoscape 2.8: New features for data integration and network visualization. Bioinformatics. 2011;27: 431–432. doi:10.1093/bioinformatics/btq675
52. Marchler-Bauer A, Bo Y, Han L, He J, Lanczycki CJ, Lu S, et al. CDD/SPARCLE: Functional classification of proteins via subfamily domain architectures. Nucleic Acids Res. 2017;45: D200–D203. doi:10.1093/nar/gkw1129
53. Sievers F, Wilm A, Dineen D, Gibson TJ, Karplus K, Li W, et al. Fast, scalable generation of high-quality protein multiple sequence alignments using Clustal Omega. Mol Syst Biol. 2011;7. doi:10.1038/msb.2011.75
54. Dinkel H, Roey K Van, Michael S, Kumar M, Uyar B, Altenberg B, et al. ELM 2016

— data update and new functionality of the eukaryotic linear motif resource. Nucleic Acids Res. 2018;44: 294–300. doi:10.1093/nar/gkv1291

55. Woodward R, Gull K. Timing of nuclear and kinetoplast DNA replication and early morphological events in the cell cycle of Trypanosoma brucei. J Cell Sci. 1990;95: 49–57.

56. Siegel TN, Hekstra DR, Cross GAM. Analysis of the Trypanosoma brucei cell cycle by quantitative DAPI imaging. Mol Biochem Parasitol. 2008;160: 171–174. doi:10.1016/j.molbiopara.2008.04.004

57. Calderano SG, Drosopoulos WC, Quaresma MM, Marques CA, Kosiyatrakul S, McCulloch R, et al. Single molecule analysis of Trypanosoma brucei DNA replication dynamics. Nucleic Acids Res. 2015;43: 2655–2665. doi:10.1093/nar/gku1389

58. Venter JC, Adams MD, Myers EW, Li PW, Mural RJ, Sutton GG, et al. The sequence of the human genome. Science. 2009;291: 1304–1351. doi:10.1126/science.1058040

59. Burgess A, Lorca T, Castro A. Quantitative Live Imaging of Endogenous DNA Replication in Mammalian Cells. PLoS One. 2012;7. doi:10.1371/journal.pone.0045726

60. Conti C, Sacca B, Herrick J, Lalou C, Pommier Y, Bensimon A. Replication Fork Velocities at Adjacent Replication Origins Are Coordinately Modified during DNA Replication in Human Cells. Int J Biol Sci. 2007;6: 569–583. doi:10.1091/mbc.E06

61. Jackson DA, Pombo A. Replicon Clusters Are Stable Units of Chromosome Structure Evidence That Nuclear Organization Contributes to the Efficient Activation and Propagation of S Phase in Human Cells. J Cell Biol. 1998;140: 1285–1295.

62. DePamphillls M, Bell SD. Genome duplication. Concepts, mechanisms, evolution, and disease. New York: Garland Science; 2011.

63. Ranjbarian F, Vodnala M, Vodnala SM, Rofougaran R, Thelander L, Hofer A. Trypanosoma brucei thymidine kinase is tandem protein consisting of two homologous parts, which together enable efficient substrate binding. J Biol Chem. 2012;287: 17628–17636. doi:10.1074/jbc.M112.340059

64. Cavanagh BL, Walker T, Norazit A, Meedeniya ACB. Thymidine analogues for tracking DNA synthesis. Molecules. 2011;16: 7980–7993. doi:10.3390/molecules16097980

65. Moses JE, Moorhouse AD. The growing applications of click chemistry. Chem Soc Rev. 2007;36: 1249–1262. doi:10.1039/b613014n

66. Aranda S, Rutishauser D, Ernfors P. Identification of a large protein network involved in epigenetic transmission in replicating DNA of embryonic stem cells. Nucleic Acids Res. 2014;42: 6972–6986. doi:10.1093/nar/gku374

67. Sherwin T, Gull K. Visualization of detyrosination along single microtubules reveals novel mechanisms of assembly during cytoskeletal duplication in trypanosomes. Cell. 1989;57: 211–221. doi:10.1016/0092-8674(89)90959-8

68. Prado F, Maya D. Regulation of replication fork advance and stability by nucleosome assembly. Genes (Basel). 2017;8. doi:10.3390/genes8020049

69. Yadav T, Whitehouse I. Replication-Coupled Nucleosome Assembly and Positioning by ATP-Dependent Chromatin-Remodeling Enzymes. Cell Rep. The

Authors; 2016;15: 715–723. doi:10.1016/j.celrep.2016.03.059
70. Gassen A, Brechtefeld D, Schandry N, Arteaga-Salas JM, Israel L, Imhof A, et al. DOT1A-dependent H3K76 methylation is required for replication regulation in Trypanosoma brucei. Nucleic Acids Res. 2012;40: 10302–10311. doi:10.1093/nar/gks801
71. Janzen CJ, Hake SB, Lowell JE, Cross GAM. Selective Di- or Trimethylation of Histone H3 Lysine 76 by Two DOT1 Homologs Is Important for Cell Cycle Regulation in Trypanosoma brucei. Mol Cell. 2006;23: 497–507. doi:10.1016/j.molcel.2006.06.027
72. Siegel TN, Kawahara T, DeGrasse JA, Janzen CJ, Horn D, Cross GAM. Acetylation of histone H4K4 is cell cycle regulated and mediated by HAT3 in Trypanosoma brucei. Mol Microbiol. 2008;67: 762–771. doi:10.1111/j.1365-2958.2007.06079.x
73. Srivastava A, Badjatia N, Lee JH, Hao B, Günzl A. An RNA polymerase II-associated TFIIF-like complex is indispensable for SL RNA gene transcription in Trypanosoma brucei. Nucleic Acids Res. 2017;46: 1695–1709. doi:10.1093/nar/gkx1198
74. Moldovan GL, Pfander B, Jentsch S. PCNA, the Maestro of the Replication Fork. Cell. 2007;129: 665–679. doi:10.1016/j.cell.2007.05.003
75. Yu C, Gan H, Han J, Zhou ZX, Jia S, Chabes A, et al. Strand-Specific Analysis Shows Protein Binding at Replication Forks and PCNA Unloading from Lagging Strands when Forks Stall. Mol Cell. Elsevier Inc.; 2014;56: 551–563. doi:10.1016/j.molcel.2014.09.017
76. Lõoke M, Maloney MF, Bell SP. Mcm10 regulates DNA replication elongation by stimulating the CMG replicative helicase. Genes Dev. 2017;31: 291–305. doi:10.1101/gad.291336.116
77. Zhu W, Ukomadu C, Jha S, Senga T, Dhar SK, Wohlschlegel J a, et al. Mcm10 and And-1 / CTF4 recruit DNA polymerase α to chromatin for initiation of DNA replication. Genes Dev. 2007; 2288–2299. doi:10.1101/gad.1585607.Mcm10
78. Vos SM, Tretter EM, Schmidt BH, Berger JM. All tangled up: how cells direct, manage and exploit topoisomerase function. Nat Rev Mol Cell Biol. Nature Publishing Group; 2011;12: 827–41. doi:10.1038/nrm3228
79. Champoux JJ. DNA T OPOISOMERASES : Structure , Function ,. Annu Rev Biochem. 2001;70: 369–413.
80. Canela A, Maman Y, Jung S, Wong N, Callen E, Day A, et al. Genome Organization Drives Chromosome Fragility. Cell. 2017; 507–521. doi:10.1016/j.cell.2017.06.034
81. Singh BN, Achary VMM, Panditi V, Sopory SK, Reddy MK. Dynamics of tobacco DNA topoisomerases II in cell cycle regulation: to manage topological constrains during replication, transcription and mitotic chromosome condensation and segregation. Plant Mol Biol. Springer Netherlands; 2017;94: 595–607. doi:10.1007/s11103-017-0626-4
82. Korolev S. Advances in structural studies of recombination mediator proteins. Biophys Chem. Elsevier B.V.; 2017;225: 27–37. doi:10.1016/j.bpc.2016.12.001
83. Dembowski JA, DeLuca NA. Selective Recruitment of Nuclear Factors to Productively Replicating Herpes Simplex Virus Genomes. PLoS Pathog. 2015;11:

1–35. doi:10.1371/journal.ppat.1004939

84. Mazin A V., Mazina OM, Bugreev D V., Rossi MJ. Rad54, the motor of homologous recombination. DNA Repair (Amst). Elsevier B.V.; 2010;9: 286–302. doi:10.1016/j.dnarep.2009.12.006

85. Li B. DNA double-strand breaks and telomeres play important roles in Trypanosoma brucei antigenic variation. Eukaryot Cell. 2015;14: 196–205. doi:10.1128/EC.00207-14

86. McCulloch R, Barry JD. A role for RAD51 and homologous recombination in Trypanosoma brucei antigenic variation. Genes Dev. 1999;13: 2875–2888. doi:10.1101/gad.13.21.2875

87. Sogo, J.M; Stahl, H;Koller, Th;Knippers R. Structure of Replicating Simian Virus 40 Minichromosomes The Replication Fork, Core Histone Segregation and Terminal Structures. J mo. 1986; 189–204.

88. MacAlpine DM, Macalpine DM, Rodriguez HK, Bell SP, Bell SP. Coordination of replication and transcription along a. Genes Dev. 2004; 3094–3105. doi:10.1101/gad.1246404.ster

89. Lubelsky Y, Prinz J a, Denapoli L, Li Y, Belsky J a, Macalpine DM. DNA replication and transcription programs respond to the same chromatin cues DNA replication and transcription programs respond to the same chromatin cues. Genome Res. 2014; 1102–1114. doi:10.1101/gr.160010.113

90. Günzl A, Bruderer T, Laufer G, Tu L, Chung H, Lee P, et al. RNA Polymerase I Transcribes Procyclin Genes and Variant Surface Glycoprotein Gene Expression Sites in Trypanosoma brucei RNA Polymerase I Transcribes Procyclin Genes and Variant Surface Glycoprotein Gene Expression Sites in Trypanosoma brucei. Eukaryot Cell. 2003;2: 542–551. doi:10.1128/EC.2.3.542

91. Marchetti MA, Tschudi C, Silva E, Ullu E. Physical and transcriptional analysis of the Trypanosoma brucei genome reveals a typical eukaryotic arrangement with close interspersion of RNA polymerase II- and III-transcribed genes. Nucleic Acids Res. 1998;26: 3591–3598. doi:10.1093/nar/26.15.3591

92. Wedel C, Förstner KU, Derr R, Siegel TN. GT-rich promoters can drive RNA pol II transcription and deposition of H2A.Z in African trypanosomes. EMBO J. 2017;36: e201695323. doi:10.15252/embj.201695323

93. Alsford S, Turner DJ, Obado SO, Sanchez-flores A, Glover L, Berriman M, et al. High-throughput phenotyping using parallel sequencing of RNA interference targets in the African trypanosome High-throughput phenotyping using parallel sequencing of RNA interference targets in the African trypanosome. Genome Res. 2011;21: 915–924. doi:10.1101/gr.115089.110

94. Archer SK, Inchaustegui D, Queiroz R, Clayton C. The cell cycle regulated transcriptome of Trypanosoma brucei. PLoS One. 2011;6. doi:10.1371/journal.pone.0018425

95. Urbaniak MD, Martin DMA, Ferguson MAJ. Global quantitative SILAC phosphoproteomics reveals differential phosphorylation is widespread between the procyclic and bloodstream form lifecycle stages of Trypanosoma brucei. J Proteome Res. 2013;12: 2233–2244. doi:10.1021/pr400086y

96. Errico A, Deshmukh K, Tanaka Y, Pozniakovsky A, Hunt T. Identification of substrates for cyclin dependent kinases. Adv Enzyme Regul. Elsevier Ltd;

2010;50: 375–399. doi:10.1016/j.advenzreg.2009.12.001

97. Chang EJ, Begum R, Chait BT, Gaasterland T. Prediction of Cyclin-Dependent Kinase Phosphorylation Substrates. PLoS One. 2007;2: e656. doi:10.1371/journal.pone.0000656

98. Johnson N, Shapiro GI. Cyclin-dependent kinases (cdks) and the DNA damage response: rationale for cdk inhibitor–chemotherapy combinations as an anticancer strategy for solid tumors. Expert Opin Ther Targets. 2010;14: 1199–1212. doi:10.1111/j.1743-6109.2008.01122.x.Endothelial

99. Durocher D, Jackson SP. The FHA domain. FEBS Lett. 2002;513: 58–66. doi:10.1016/S0014-5793(01)03294-X

100. Neuwald AF. Evolutionary clues to eukaryotic DNA clamp-loading mechanisms : analysis of the functional constraints imposed on replication factor C AAA + ATPases. Nucleic Acids Res. 2005;33: 3614–3628. doi:10.1093/nar/gki674

101. Johnson A, Yao NY, Bowman GD, Kuriyan J, Donnell MO. The Replication Factor C Clamp Loader Requires Arginine Finger Sensors to Drive DNA Binding and Proliferating Cell Nuclear Antigen Loading. J Biol Chem. 2006;281: 35531–35543. doi:10.1074/jbc.M606090200

102. Kim J, MacNeill SA. Genome Stability: A New Member of the RFC family. Curr Biol. 2003;13: 873–875. doi:10.1016/j.cub.2003.10.048

103. Shiomi Y, Nishitani H. Control of genome integrity by RFC complexes; conductors of PCNA loading onto and unloading from chromatin during DNA replication. Genes (Basel). 2017;8. doi:10.3390/genes8020052

104. Shiomi Y, Hayashi A, Ishii T, Shinmyozu K, Nakayama J -i., Sugasawa K, et al. Two Different Replication Factor C Proteins, Ctf18 and RFC1, Separately Control PCNA-CRL4Cdt2-Mediated Cdt1 Proteolysis during S Phase and following UV Irradiation. Mol Cell Biol. 2012;32: 2279–2288. doi:10.1128/MCB.06506-11

105. Yao NY, Donnell MO. The RFC Clamp Loader: Structure and Function. Subcell Biochem. 2012;62: 259–279. doi:10.1007/978-94-007-4572-8

106. Hanna JS, Kroll ES, Lundblad V, Spencer F a. Saccharomyces cerevisiae CTF18 and CTF4 are required for sister chromatid cohesion. Mol Cell Biol. 2001;21: 3144–3158. doi:10.1128/MCB.21.9.3144-3158.2001

107. Aroya S Ben, Kupiec M. The Elg1 replication factor C-like complex: A novel guardian of genome stability. DNA Repair (Amst). 2005;4: 409–417. doi:10.1016/j.dnarep.2004.08.003

108. Zou L, Cortez D, Elledge SJ. Regulation of ATR substrate selection by Rad17-dependent loading of Rad9 complexes onto chromatin. Genes Dev. 2002;16: 198–208. doi:10.1101/gad.950302

109. Hammarton TC, Clark J, Douglas F, Boshart M, Mottram JC. Stage-specific differences in cell cycle control in Trypanosoma brucei revealed by RNA interference of a mitotic cyclin. J Biol Chem. 2003;278: 22877–22886. doi:10.1074/jbc.M300813200

110. Li Z, Wang CC. A PHO80-like cyclin and a B-type cyclin control the cell cycle of the procyclic form of Trypanosoma brucei. J Biol Chem. 2003;278: 20652–20658. doi:10.1074/jbc.M301635200

111. Tu X, Wang CC. The Involvement of Two cdc2-related Kinases (CRKs) in Trypanosoma brucei Cell Cycle Regulation and the Distinctive Stage-specific

Phenotypes Caused by CRK3 Depletion. J Biol Chem. 2004;279: 20519–20528. doi:10.1074/jbc.M312862200

112. Ploubidou a, Robinson DR, Docherty RC, Ogbadoyi EO, Gull K. Evidence for novel cell cycle checkpoints in trypanosomes: kinetoplast segregation and cytokinesis in the absence of mitosis. J Cell Sci. 1999;112 (Pt 2: 4641–4650.

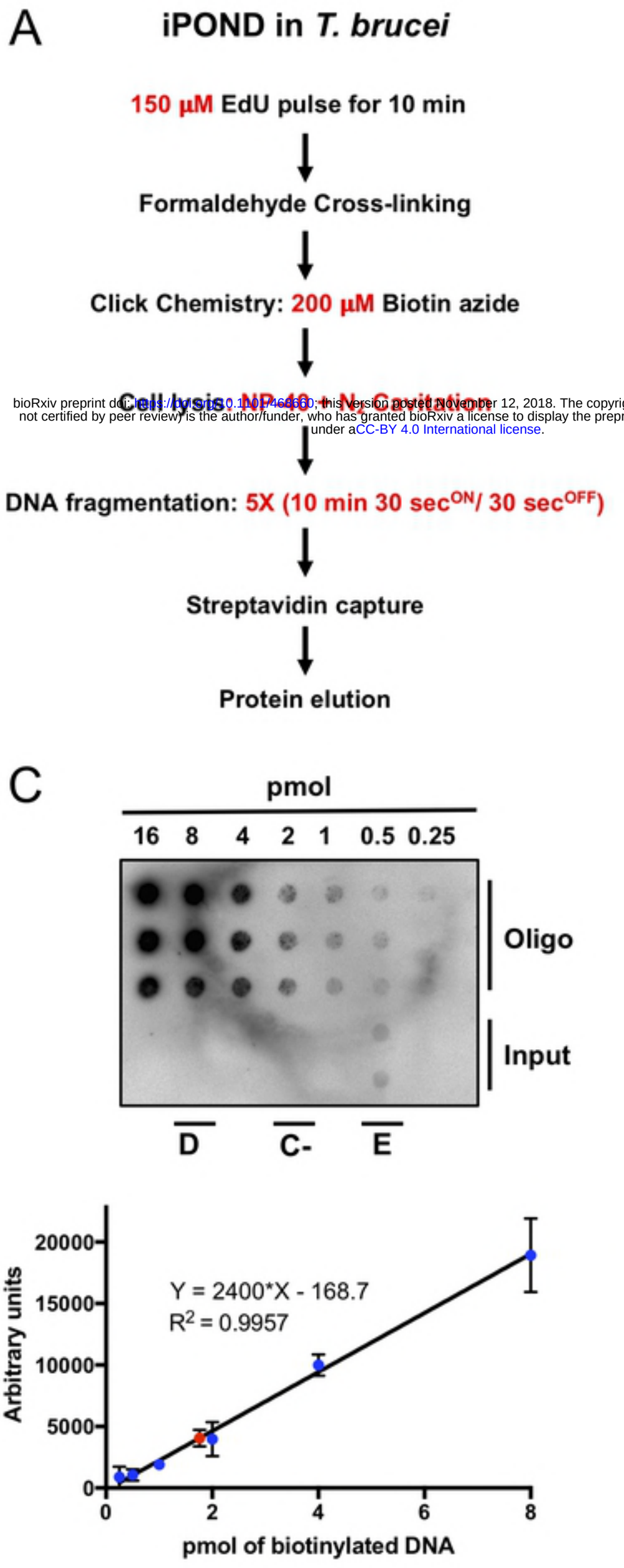

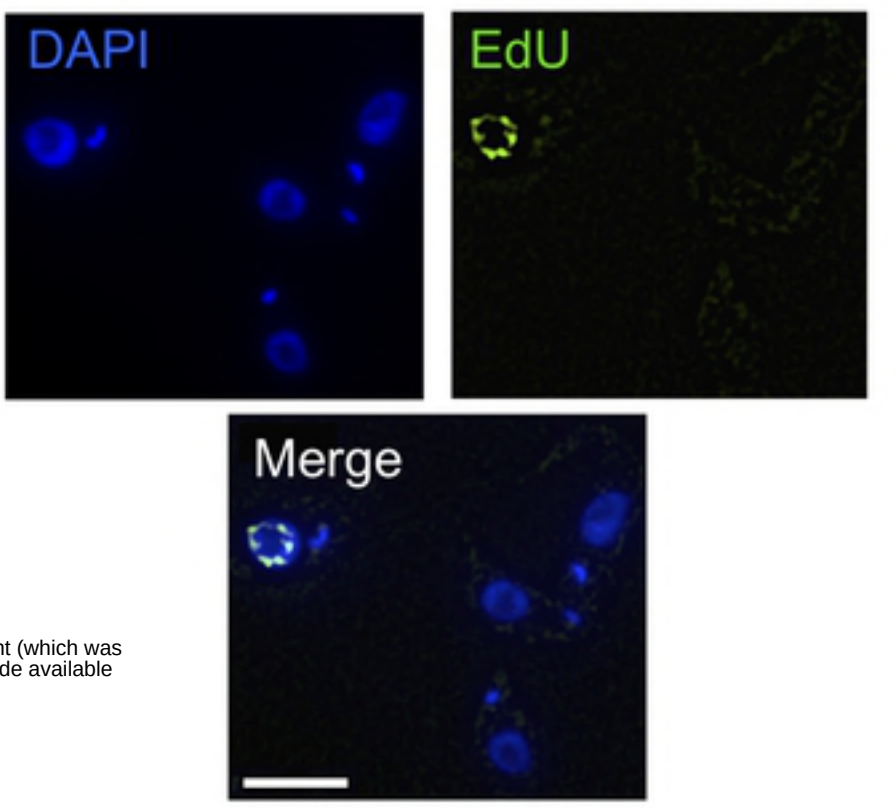

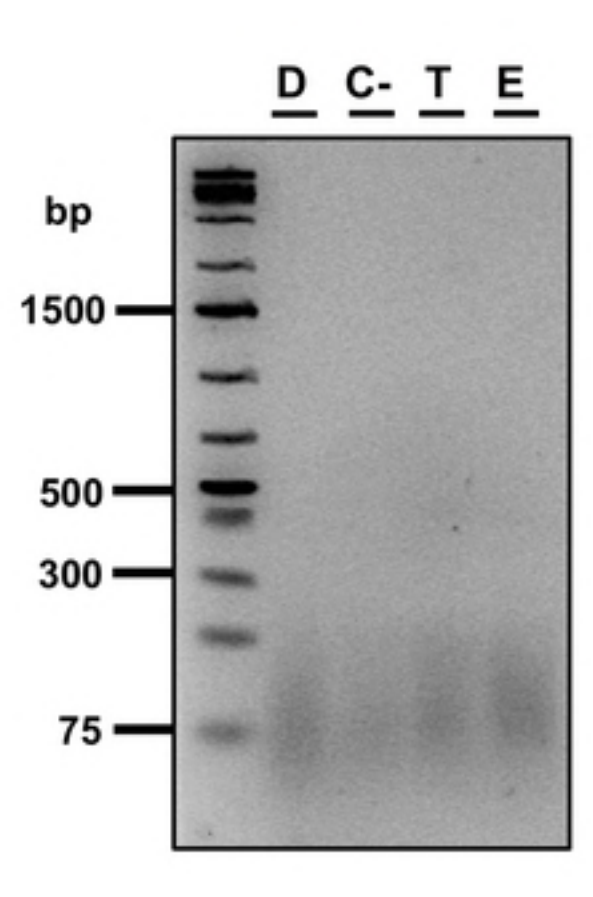

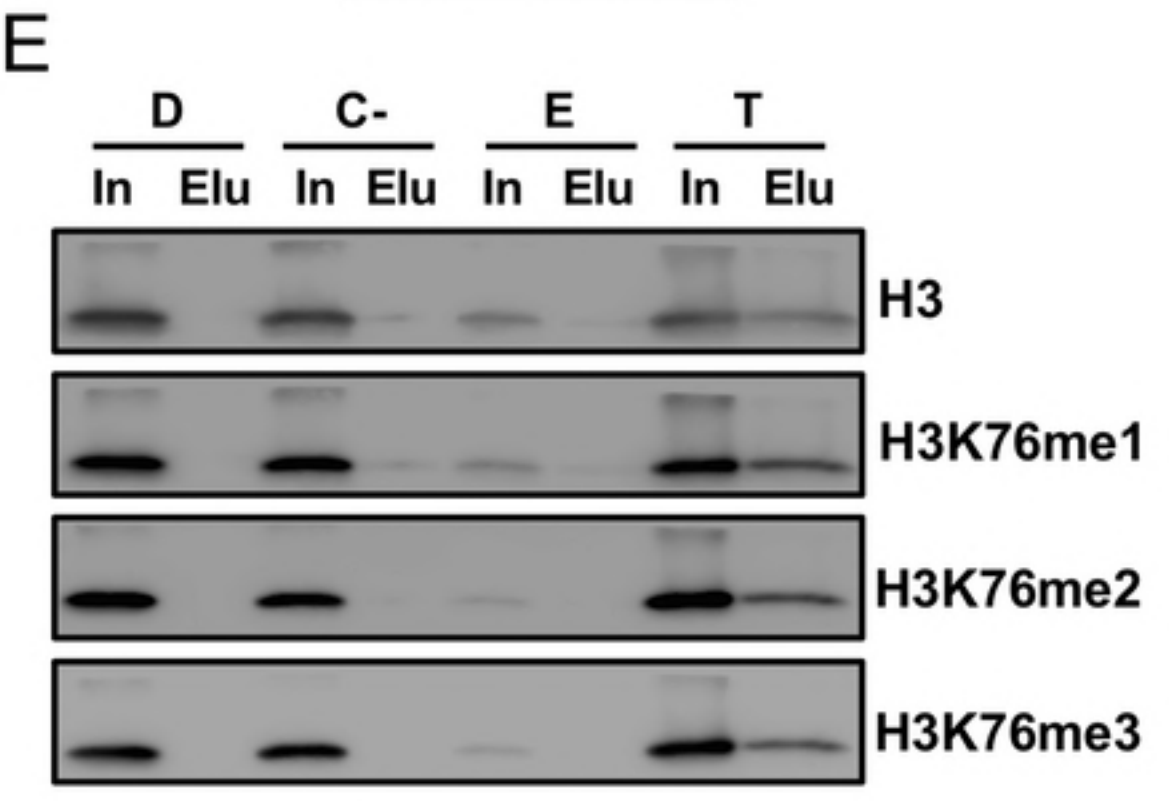

Figure 1

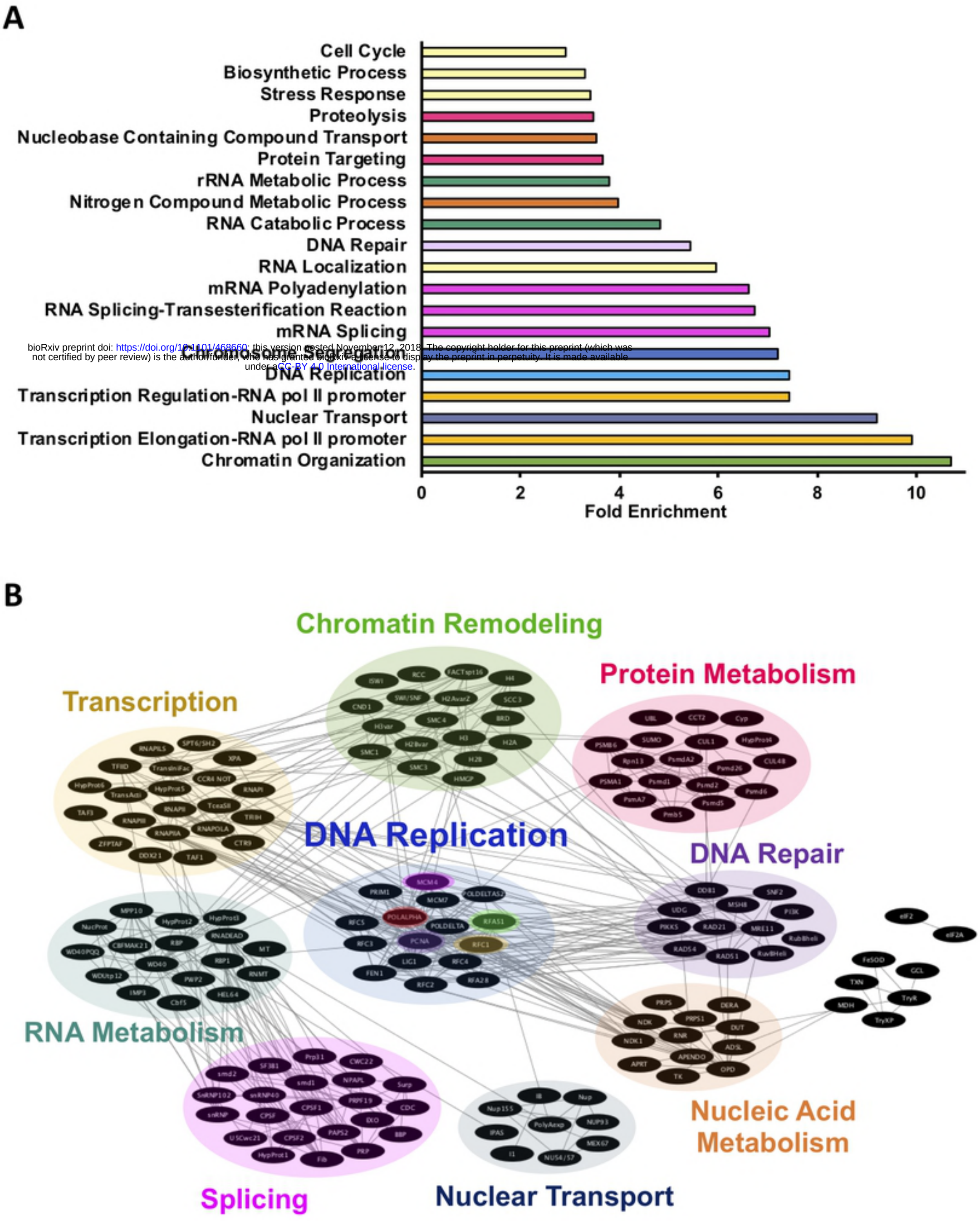

Figure 2

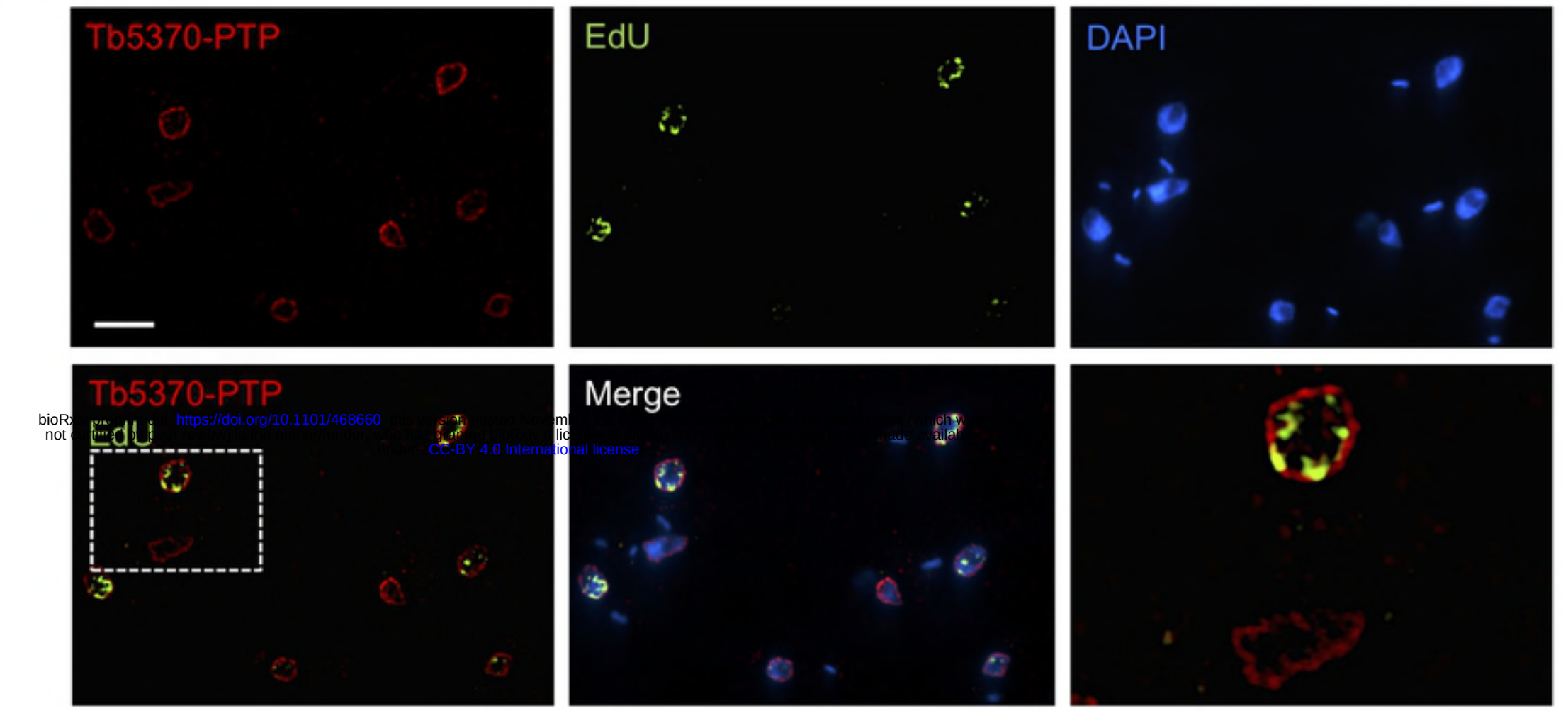

Figure 3

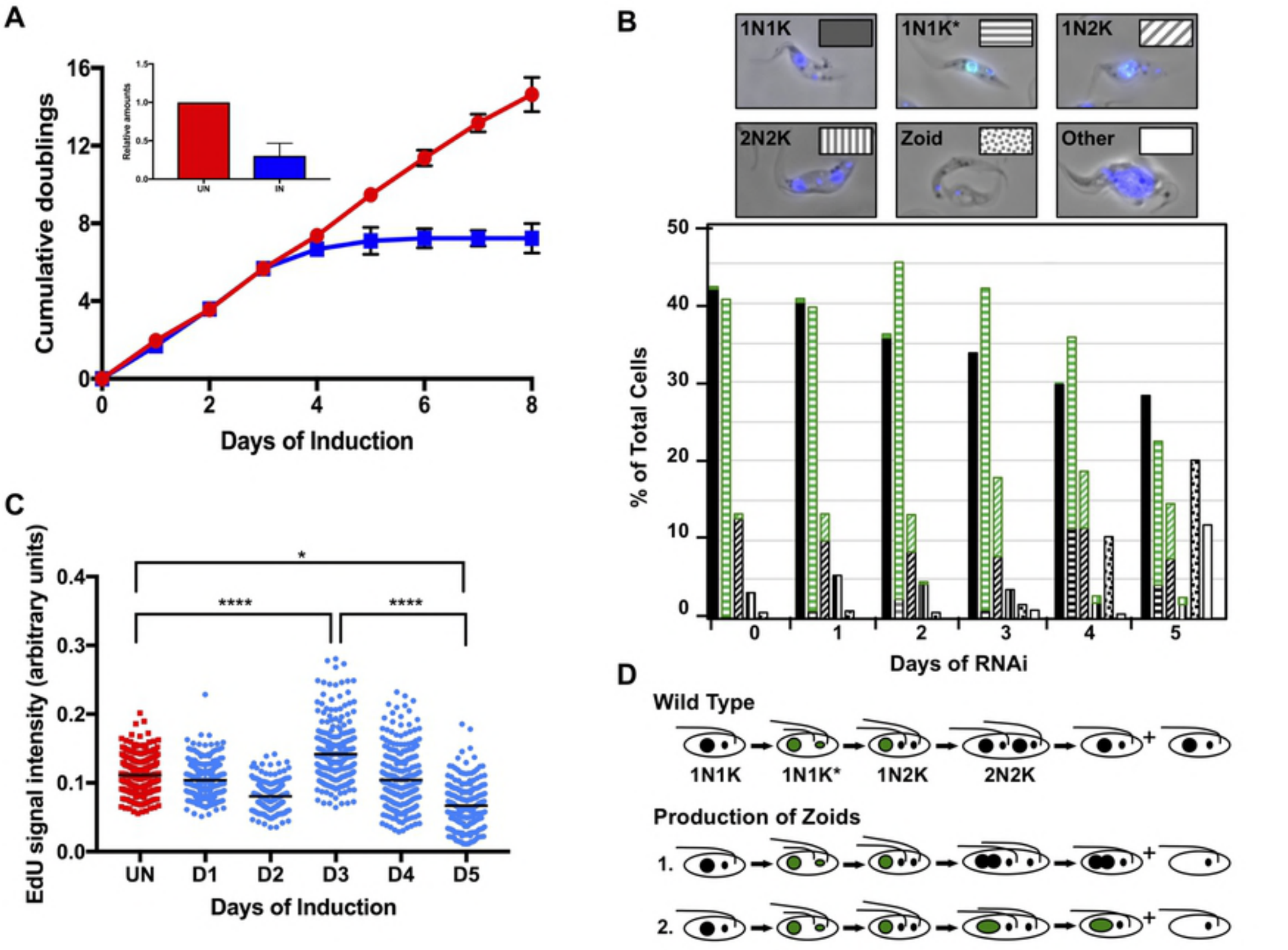
A
Cumulative doublings
Days of Induction
Relative amounts
UN
IN
B
1N1K
1N1K*
1N2K
2N2K
Zoid
Other
% of Total Cells
Days of RNAi
C
EdU signal intensity (arbitrary units)
UN
D1
D2
D3
D4
D5
Days of Induction
****
****
*
D
Wild Type
1N1K
1N1K*
1N2K
2N2K
Production of Zoids
1.
2.

Figure 4